Leonardo dos Santos Ferreira

Dynamics of the Ising model on heterogeneous random graphs with arbitrary threshold noise

Porto Alegre, RS - Brasil
July 4, 2023

Leonardo dos Santos Ferreira

Dinâmica do modelo de Ising fora do equilíbrio sobre redes complexas heterogêneas com distribuição de ruído arbitrária

Dissertação realizada sob a orientação do Prof. Dr. Fernando Lucas Metz e apresentada ao Instituto de Física da UFRGS, em preenchimento parcial dos requisitos para a obtenção do título de Mestre em Física.

Universidade Federal do Rio Grande do Sul – UFRGS
Instituto de Física
Programa de Pós-Graduação

Orientador: Prof. Dr. Fernando Lucas Metz

Porto Alegre, RS - Brasil
4 de abril, 2023

Acknowledgements

First, I thank my parents and friends for making bearable the tragic mockery that is life. Second, I thank my advisor, for the lessons and for the camaradarie. They made easier to endure through such a stressfull period. Finally, I thank CAPES for the financial support, under the finance code 001.

Abstract

Key-words: Ising model, non-equilibrium, complex networks.

Collective phenomena in complex networks are very important in modern science. Meanwhile analytical studies in this area are limited to homogêneous networks, where the number of connections per node is constant, real complex networks are heterogeneous and, therefore, their investigation is made mainly through numerical simulations and data science techniques. In this work, we analyticaly solve the parallel dynamics of the Ising model on an ensemble of complex networks with an aribitrary distribution in the number of conections per node, valid in the high connectivity limit. Depending on the threshold noise distribution, that mimics the effect of the heat bath, the system can evolve to non equilibrium stationary states, since the explicit form of the threshold noise distribution determines the distribution of microscopic states. Our main result is a pair of equations that describe the dynamics of the global magnetization of the system, in terms of the degree and threshold noise distributions. In the long time limit, these equations allow to determine the critical temperature for the continuous transtition between ferromagnetic and paramagnetic phases. We show that the critical temperature is determined by the variance of the degree distribution and by the behavior of the threhsold noise distribution near zero. The focus of this work lies in the calculation of the critical exponents, both stationary and dynamical, for the global magnetization and for the variance of the distribution of local magnetizations, in the case which the degrees follow a negativa binomial distribution. This choice is convenient because it allows to parametrize the heterogeneity of the network in terms of a single paramenter. For a hyperbolic tangent threshold noise noise distribution, that promotes detailed balance, both stationary and dynamical critical exponents agree with previous results from the usual homogeneous mean field theories. For an algebraic threshold noise distribution, however, detailed balance is broken and the critical exponents are determined by the tails of the threshold noise distribution. Finally, we shot that, as the systems approaches the critical temperature, the relaxation time for the magnetization inside each phase diverges according to typical values of the homegeneous mean-field theory regardless of the threshold noise distribution. With these results, we highlight the importance of the degree and termal noise fluctuations on the dynamics of the Ising model, presenting one step further on the direction of the understanding of the theoretical description of real complex network phenomena. Generally, we show that the critical exponents do not depend on the heterogeneity of the network, depending only on the threshold noise distribution.

Resumo

Palavras-chaves: Modelo de Ising, não-equilíbrio, redes complexas.

Fenômenos coletivos em redes complexas vem se tornando cada vez mais importantes na ciência moderna. Enquanto estudos analíticos nesta área se limitam essencialmente à redes homogêneas, onde o número de conexões por nó não varia, redes complexas reais são heterogêneas e, portanto, seu estudo é feito principalmente através de técnicas de simulação e análise de dados. Neste trabalho, resolvemos analiticamente a dinâmica paralela do modelo de Ising em um ensemble de redes complexas com uma distribuição arbitrária no número de conexões por sítio, valida no limite de alta conectividade. Dependendo da distribuição de ruído de limiar, que mimetiza o efeito do banho térmico, o sistema pode evoluir para estados estacionários de não equilíbrio, uma vez que a forma explícita da distribuição de ruído de limiar determina a forma da distribuição de estados microscópicos. Nosso resultado principal é um par de equações que descreve a dinâmica da magnetização global do sistema em termos das distribuições de grau e de ruído de limiar. No limite de tempos longos, essas equações permitem determinar a temperatura crítica da transição contínua entre as fases ferromagnética e paramagnética. Mostramos que a temperatura crítica depende da variância da distribuição de graus e do comportamento da distribuição do ruído de limiar próxima a zero. O foco deste trabalho está no cálculo dos expoentes críticos, tanto estacionários quanto dinâmicos, para a magnetização global e para a variância da distribuição das magnetizações locais, no caso em que os graus seguem uma distribuição binomial negativa. Esta escolha da distribuição de graus é conveniente pois permite parametrizar a heterogeneidade da rede em termos de um único parâmetro. Para uma distribuição de ruído de limiar dada por uma tangente hiperbólica, que promove balanço detalhado, os expoentes críticos estacionários e dinâmicos da magnetização assumem os valores usuais da teoria de campo médio homogênea. Já para uma distribuição de ruído algébrica, o balanço detalhado é quebrado, e os expoentes críticos são determinados pela cauda da distribuição de ruído de limiar. Por fim, mostramos que, a medida que o sistema se aproxima da temperatura crítica, o tempo de relaxação da magnetização em cada fase diverge de acordo com valores típicos de teorias de campo médio homogêneas independentemente da distribuição de ruído de fundo. Com esses resultados, evidenciamos a importância das flutuações de grau e de ruído térmico na dinâmica do modelo de Ising, dando um passo a mais na direção da descrição teórica de modelos em redes complexas reais. Em geral, nós mostramos que os expoentes críticos não dependem da heterogeneidade da rede, mas dependem apenas da distribuição de ruído de limiar.

Contents

1 Introduction

In recent years, scientists have gained access to an extraordinary amount of data. From the necessity to process and analyze such large quantity of informatiom different fields, such as medicine [1], sports analytics [2] and astronomy [3], the discipline of Data Science naturally emerged with the establishment of the so called "big data era". Interestingly, statistical physics found in this data revolution a large number of new applications [4], providing a wide set of tools for data and computer scientists, such as the concepts of phase transitions and energy landscapes in the context of complex systems. While the standard approach of data science is to develop learning algorithms to correctly predict new observations by training models from a given dataset [5], the main contribution of statistical physics to this new plethora of problems comes in the form of simplified systems, whose solution may reproduce a particular feature of the observations and provides phenomenological intuition about real phenomena.

Complex systems are ubiquitous in modern science, and may be defined as systems with a large collection of interacting units, whose behavior crucially dependends on its details [6], presenting rich phenomena such as collective behavior and phase transitions. Even though the intricate interaction between their microscopic constituints make complex systems very hard to model, they present the astonishing property of universal critical behavior [7]. Examples of complex systems can be found in neuroscience, when studying the activation of about fifty billion neurons in the cortex of the human brain [8]; in sociology, where the dynamics of opinion formation depends on the communication of a large number of individuals [9]; or in meteorology, where the intricate dynamics of the earth's climate depends on properties across diferent space and temporal scales [10]. While data science develops methods to predict meteorological conditions based on present and past observations, or models neuronal activation profiles based on measurements of brain activity, the typical approach of a physicist is to conceive minimal models to reproduce specific aspects of the observations. This approach led, for instance, to the development of energy balance models for global temperature [11] and to the Wilson-Cowan equations for biological neural networks [12]. Clearly, physical models are improved based on what is learned from real data, as we have seen in the recent development of disease evolution for the COVID-19 pandemic evidences [13]. In short, this modelling approach differs from the predictive approach of data science, as the former is focused on phenomenological intuition.

Complex systems can be represented through a complex network, a simplified representation that reduces a system to an abstract structure capturing only the basic information regarding the interaction between individuals [14]. Complex networks are defined in terms of a set of nodes connected by links, and are known in math as random graphs [15]. A

node may represent a person in a community [16], a species in a food web [17] or an economic agent in a market [18], and interacts with neighboring nodes through its links. The nature of the interactions also depends on the context. The links can model a social pressure towards a given choice (an individual may vote for candidate A or B based on the vote of its connections), the status of an ecological relationship between species (species A feeds on B that feeds on C) or the balance of a wealth exchange between agents (which node benefits in a win-lose pair wise exchange). Even though complex networks are simplifications of complex systems, they capture their central aspects, such as emergent collective behavior and phase transitions. From the microscopic local interactions, global macroscopic features may emerge, generating the perfect scenario to the application of statistical mechanics. For instance, a social system may evolve to a global opinion profile, where a macroscopic fraction of the population votes for candidate A instead of B [19], or a dynamical macroscopic activation pattern may arise in the neuronal population forming the human cortex [20]. Since the nature of the macroscopic behavior depends on a set of model parameters of the model, the machinery developed to study phase transitions in physical systems can describe macroscopic properties of complex systems.

Equilibrium statistical physics describes systems in thermodynamic equilibrium [21]. In such cases, the relaxation from an initial configuration to a stationary state leads to the occupation of the available microstates, which are distributed according to the Boltzmann distribution. However, the relaxation mechanism still lacks a general theory. Also, the application of statistical physics to other areas is highlighting systems for which detailed balance may not hold, resulting in the occupation of microstates distributed in discordance with the Boltzmann distribution [22]. Therefore, even the stationary configuration, such systems will not be in thermal equilibrium. The description of these two different situations is the central aim of non-equilibrium statistical physics, and complex systems are a fruitful scenario for their investigation.

Mean-field theories in statistical physics are important because they capture collective phenomena and phase transitions in complex systems [7]. In a mean field approach, each individual interacts with a coarse-grained effective field produced by its neighbors, instead of taking into account the detailed contribution of each individual variable. Averaging the behaviour of an individual over this effective field provides a macroscopic description of the system in terms of order parameters, which captures qualitative features of phase transitions [23]. Within the context of mean-field theories, the Ising model stands out for its simplicity. Introduced as a model of magnetic materials [24, 25], the Ising model is formed by a set of binary random variables with values plus or minus one, called spins, placed at each node of a network. The spins interact with each other through the coupling strenght associated to each link and the state of a node depends on the configuration of its neighbors. Interestingly, many different systems and problems can be mapped onto the Ising spins, so the model is a minimal framework to study problems from many different

areas, such as sociology [19], economy [26] and computer science [27]. The coupling determines both the strength and the nature of the interaction. If the interaction between two spins is positive, they tend to point in the same direction, while if it is negatie, the tend to point in contrary directions. The coupling strenghts can also introduce interaction disorder in the system. By assuming that the coupling follow from a symmetric probability distribution, the coexistence of ferromagnetic (positive couplings) and anti-ferromagnetic (negative couplings) interactions is promoted. One famous example of a disordered spin model is the Sherrington-Kirkpatrick spin glass [28], where the couplings between spins are drawn from a Gaussian distribution, leading to many interesting phenomena [29].

Another kind of disorder may arise from the structure of the underlying network. For instance, we can consider the ferromagnetic Ising model on a two-dimensional lattice [30] and randomly remove some of the connections between the spins. In this new model, known as diluted two-dimensional lattice [31], the Ising ferromagnet may behave drastically different than in the original two-dimensional model. The diluted two dimensional lattice is one example of model in which the number of conections per spin, or degree of each spin, is random. Another important example of network with degree fluctuations is the Erdős-Réniy ensemble [15], where a probability is assigned to each possible pair of spins to be connected. While most models consider homogeneous networks, where degree fluctuations are irrelevant, and must resort to the thermodynamic limit in order to provide analytical solutions, real complex networks are sparse and heterogeneous, *i.e.*, present finite connectivity and degree fluctuations. For these reasons, the investigation of real phenomena is heavily based on numerical simulations and data science methods, so the analytical understanding of the effects of network heterogeneities in spin models is a central problem in network science [32].

Concerning equilibrium critical phenomena, Ising models are characterized by well known mean-field critical exponents, as long as the fourth moment of the degree distribution is finite [33–35], even in heterogeneous networks [36]. In comparison with complex systems that evolve to an equilibrium behavior, progress has been much slower on the side of non-equilibrium heterogeneous Ising models, both dynamical and stationary. To the best of our knowledge, the stationary non-equilibrium critical exponents are not known. Another challenge regarding non-equilibrium Ising models is that, in contrast to the majority of problems of classical mechanics [37], Ising systems lack an intrinsic dynamics. This is due to the fact that they are described by a pseudohamiltonian [38], devoid of a set of natural equations of motion generally derived through Hamilton's relations. Therefore, the evolution rule for Ising systems must be set up artificially. The most common update scheme for the Ising model is called Glauber dynamics [39], where the spins are updated based on the local fields induced by the configuration of their neighbours, plus a stochastic threshold noise that mimics the contact with a heat bath. Since detailed balance fails depending on the distribution of the threshold noise [40], the explicit form of the distri-

bution plays a main role on the characterization of stationary limits as equilibrium or non equilibrium states. The effects of degree and thermal fluctuations on the dynamical exponents [54] are also not known.

There are two main classes of networks for which the dynamics of Ising spins is solved: dense random graphs and sparse directed random graphs [41–43]. Interestingly, recent studies on the spectra of random graphs [44] and on the equilibrium of spin models on networks [36] led to analytical solutions that depend on the degree distribution, in the limit where the mean degree is infinitely large. In this work, we extend these previous results to the non-equilibrium dynamics of the Ising model. By considering ferromagnetic couplings, we develop a mean field theory that describes the evolution of the Ising models for arbitrary degree and threshold noise distributions. Our results improve the understanding of critical phenomena of Ising systems in highly connected networks, being one step closer to the description of real sparse complex networks, accessible only through simulations. In addition, we generalize the aforementioned works by considering distributions of threshold noise that induce the breakdown of detailed balance, presenting an analytical framework that has potential applications beyond physical systems. Overall, our work introduces the Ising models on a class of networks that retain the effect of both topological structure and noise distribution, whose non-equilibrium dynamics can be solved exactly, presenting insights on the network and termal fluctuations effects on the Ising model.

This work is organized as follows. In the first part of Chapter 2, we introduce the Ising model and present the microscopic dynamics known as Glauber parallel dynamics. Then, we derive the probabilistic version of the dynamics and proceed to the derivation of the dynamical equations for the global and local magnetizations of the heterogeneous Ising model with arbitrary threshold noise distribution. In Chapter 3 we explore in detail the consequences of the dynamical equations by choosing the negative binomial degree distribution, that allow to easily interpolate between homogeneous and heterogeneous networks, and by comparing two different threshold noise distributions, one for which detailed balance holds and one for which it does not. We derive both stationary and dynamical critical exponents and discuss their dependence on degree and thermal fluctuations. In the last chapter, we conclude the work by presenting a concise review of the results and pointing some interesting open questions in the field.

2 Stochastic dynamics of the Ising model

The Ising model was introduced by Wilhelm Lenz and Ernst Ising (1920 [24] and 1925 [25], respectively) as a modelling tool to understand equilibrium ferromagnetism. It is a simplified model that treats the atomic magnetic moments as binary variables, or spins, that interact in order to minimize the system's energy. Beyond its original physical motivation, a myriad of modern applications raised the Ising model to the level of a general framework to study complex systems, such as algorithm optimization [27], opinion formation [19] and economy stability [26]. The Ising model consists of a collection of N spins $\sigma_i = \pm 1$, identified by the index $i = 1, \cdots, N$, whose equilibrium configuration is described by the Boltzmann distribution [45]

$$p(\boldsymbol{\sigma}) = e^{-\beta H(\boldsymbol{\sigma})}, \tag{2.1}$$

where β is the inverse temperature parameter and $H(\boldsymbol{\sigma})$ is the hamiltonian of the system, given by

$$H(\boldsymbol{\sigma}) = -\sum_{(i,j)} J_{ij}\sigma_i\sigma_j. \tag{2.2}$$

In equation (2.2), $\sum_{(i,j)}$ denotes summation over all pairs of interacting spins and J_{ij} is a coupling factor, which controls the strength and nature of the pairwise interaction. A pair of spins tend to align for ferromagnetic $J_{ij} > 0$ and anti-align for anti-ferromagnetic $J_{ij} < 0$ couplings.

An important aspect of the Ising model is that it has no intrinsic dynamics. As discussed in [38], this results from the fact that equation (2.2) is actually a pseudohamiltonian, devoid of a set of natural equations for the evolution of its generalized coordinates and associated momenta. A simple artificial dynamical rule to describe the microscopic evolution of an Ising system was proposed by Roy Glauber in 1963 [39]. It consists of updating spins at integer time steps t based on the equation

$$\sigma_{i,t+1} = \mathrm{sgn}[h_i(\boldsymbol{\sigma}_t) + T\zeta_{i,t}], \tag{2.3}$$

where the vector $\boldsymbol{\sigma}_t$ denotes the microstate of the system at time t and $\zeta_{i,t}$ are independent and identically distributed random variables drawn from a probability distribution $\mu(\zeta)$. The quantities ζ define the threshold noise that mimics the heat bath. The sign function $\mathrm{sgn}[x]$ is defined as

$$\mathrm{sgn}[x] = \begin{cases} 1, \text{ if } x > 0, \\ -1, \text{ if } x < 0, \end{cases} \tag{2.4}$$

and $h_i(\boldsymbol{\sigma}_t)$ is the local field at site i and time t, given by

$$h_i(\boldsymbol{\sigma}_t) = \sum_{j=1}^{N} J_{ij}\sigma_{j,t}. \tag{2.5}$$

The local fields introduce correlation between spins and define a mechanism through which a spin evolves based on its interaction with the neighborhood. For $T \to 0$, the dynamics is completely deterministic, while for $T \to \infty$ it is completely random since the stochastic term in (2.3) dominates the sign function, rendering correlation between spins introduced by (2.5) irrelevant.

The remainder of this chapter is divided as follows. In Section 2.1, we derive a probabilistic description of the updating rule (2.3) in the case of parallel dynamics, and discuss the relation between the threshold noise distribution $\mu(\zeta)$ and detailed balance. In Section (2.2), we address the effects of structural disorder on the system and present the dynamical equations for the ferromagnetic Ising model on random graphs. Finally, in Section (2.3) we introduce the notion of critical exponents and present a brief review of such exponents regarding the Ising model.

2.1 Probabilistic description of parallel microscopic dynamics

In the first part of this chapter we presented the so called Glauber dynamics, defined by equation (2.3). There are two main ways to apply this evolution rule [45]: one could choose randomly a single spin $\sigma_{i,t}$ at each time step and update it, simulating a continuous time process (as it was done originally in [39]), or update all spins simultaneously, generating a discrete time process. Each of these possibilities is referred to in the literature as sequential and parallel evolution, respectively. In this work, we consider the latter case, *i.e.*, at each time step all spins are simultaneously updated based on the configuration of the system on the previous time step. Since each parallel iteration counts for up to N sequential steps, the discrete time evolution captures the long time behavior of the system, and even though a continuous time approach would be closer to physical reality, such discrete approach has applications on fundamental optimization problems in computer science [27].

Parallel dynamics can be described in terms of probabilities, which is more suitable for an analytical development based on the microscopic probability $p_t(\boldsymbol{\sigma})$ of observing a global configuration $\boldsymbol{\sigma}$ at a time t. Since the microscopic dynamics is a Markov process, the time evolution of $p_t(\boldsymbol{\sigma})$ follows from

$$p_{t+1}(\boldsymbol{\sigma}) = \sum_{\boldsymbol{\sigma}'} W(\boldsymbol{\sigma}|\boldsymbol{\sigma}')p_t(\boldsymbol{\sigma}'), \tag{2.6}$$

where $W(\boldsymbol{\sigma}|\boldsymbol{\sigma}')$ is the transition probability from state $\boldsymbol{\sigma}'$ to $\boldsymbol{\sigma}$. We stress that the transition probabilities are not functions of time, only of the state configurations, and once an initial probability $p_0(\boldsymbol{\sigma})$ is given, what we need is to determine the explicit form of such transition probabilities in order to solve the dynamics.

Let us derive $W(\boldsymbol{\sigma}|\boldsymbol{\sigma}')$ from equation (2.3). Considering the transition from a microstate $\boldsymbol{\sigma}'$ to another $\boldsymbol{\sigma}$, the updating rule can be formulated as

$$\sigma_{i,t+1} = \begin{cases} 1, & \text{if } \zeta_{i,t} > -\beta h_i(\boldsymbol{\sigma}'_t), \\ -1, & \text{if } \zeta_{i,t} < -\beta h_i(\boldsymbol{\sigma}'_t), \end{cases} \tag{2.7}$$

where $\beta = 1/T$ is the inverse temperature parameter. Each of the possible transitions happens with probability

$$p(\sigma_{i,t+1} = 1) = \int_{-\beta h_i(\boldsymbol{\sigma}'_t)}^{\infty} d\zeta \mu(\zeta), \tag{2.8}$$

$$p(\sigma_{i,t+1} = -1) = \int_{-\infty}^{-\beta h_i(\boldsymbol{\sigma}'_t)} d\zeta \mu(\zeta). \tag{2.9}$$

Assuming a symmetric threshold noise distribution, $\mu(\zeta) = \mu(-\zeta)$, the probability $p(\sigma_{i,t+1} = 1)$ can be written as

$$p(\sigma_{i,t+1} = 1) = \int_{\beta h_i(\boldsymbol{\sigma}'_t)}^{\infty} d\zeta \mu(\zeta) + \mathcal{F}\left[\beta h_i(\boldsymbol{\sigma}'_t)\right], \tag{2.10}$$

where

$$\mathcal{F}\left[\beta h_i(\boldsymbol{\sigma}'_t)\right] = \int_{-\beta h_i(\boldsymbol{\sigma}'_t)}^{\beta h_i(\boldsymbol{\sigma}'_t)} d\zeta \mu(\zeta) = 2\int_{0}^{\beta h_i(\boldsymbol{\sigma}'_t)} d\zeta \mu(\zeta) \tag{2.11}$$

is the so called activation function. Combining equations (2.9) and (2.10), we can drop the time index and write as unique equation for the transition probability of a single spin as follows

$$W(\sigma_i|\boldsymbol{\sigma}') = \delta_{\sigma_i,1}\left[\int_{\beta h_i(\boldsymbol{\sigma}')}^{\infty} d\zeta \mu(\zeta) + \mathcal{F}[\beta h_i(\boldsymbol{\sigma}')]\right] + \delta_{\sigma_i,-1}\int_{-\infty}^{-\beta h_i(\boldsymbol{\sigma}')} d\zeta \mu(\zeta). \tag{2.12}$$

Making use of the fact that $W(\sigma_i|\boldsymbol{\sigma}')$ must be normalized and of the identity $\delta_{\sigma,\pm 1} = \frac{1}{2}(1 \pm \sigma)$, we obtain the compact form

$$W(\sigma_i|\boldsymbol{\sigma}') = \frac{1}{2}\{1 + \sigma_i \mathcal{F}[\beta h_i(\boldsymbol{\sigma}')]\}. \tag{2.13}$$

From equation (2.13), since each spin is updated in parallel, we obtain the explicit form for the transition probability

$$W(\boldsymbol{\sigma}|\boldsymbol{\sigma}') = \prod_{i=1}^{N} \frac{1}{2}\{1 + \sigma_i \mathcal{F}[\beta h_i(\boldsymbol{\sigma}')]\}, \tag{2.14}$$

allowing to write equation (2.6) in terms of the activation function as

$$p_{t+1}(\boldsymbol{\sigma}) = \sum_{\boldsymbol{\sigma}'} p_t(\boldsymbol{\sigma}') \prod_{i=1}^{N} \frac{1}{2}\{1 + \sigma_i \mathcal{F}[\beta h_i(\boldsymbol{\sigma}')]\}. \tag{2.15}$$

This last result is the probabilistic version of (2.3). Once an initial probability $p_0(\boldsymbol{\sigma})$ is given, it establishes a recurrence relation for the probabilistic evolution of the system. Differentiating equation (2.11) with respect to $\beta h_i(\boldsymbol{\sigma}') = x$, we have

$$\frac{1}{2}\frac{d\mathcal{F}(x)}{dx} = \frac{d}{dx}\int_0^x d\zeta \mu(\zeta), \tag{2.16}$$

so we can make use of the fundamental theorem of calculus to establish the relation between the activation function and the distribution $\mu(\zeta)$ of the threshold noise as

$$\mu(x) = \frac{1}{2}\frac{d\mathcal{F}(x)}{dx}. \tag{2.17}$$

In addition, equation (2.11) leads to important properties of the activation function, namely

$$\mathcal{F}(x) = -\mathcal{F}(x), \quad \lim_{x\to\pm\infty} \mathcal{F}(x) = \pm 1. \tag{2.18}$$

Equation (2.15) is the starting point to solve the dynamics on random graphs, presented in the next section. This equation establishes that the dynamics is completely described by the threshold noise $\mu(\zeta)$ in terms of the activation function $\mathcal{F}[\beta h_i(\boldsymbol{\sigma})]$, whose explicit form is related to the maintenance of detailed balance. When the Ising model evolving through parallel dynamics obeys detailed balance, the stationary microscopic probability has the Boltzmann form [45]

$$p(\boldsymbol{\sigma}) = \frac{1}{Z}\prod_{i=1}^{N} \cosh(\beta h_i(\boldsymbol{\sigma})), \tag{2.19}$$

where Z is the partition function. In general, this result does not hold for any choice of $\mathcal{F}[\beta h_i(\boldsymbol{\sigma})]$, strongly suggesting that detailed balance fails in such cases. Therefore, in Chapter 3 we will explore the effects of two different choices of activation function, one for which equation (2.19) holds, and one for which it does not hold.

2.2 Solution for highly connected random graphs

In this section, we will derive a closed set of dynamical equations that describe the evolution of the global magnetization at time t, given by

$$m_t = \lim_{N\to\infty} \frac{1}{N}\sum_{i=1}^{N} m_{i,t}. \tag{2.20}$$

The local magnetization at node i and time t reads

$$m_{i,t} = \sum_{\sigma\in\{-1,1\}} \sigma p_{i,t}(\sigma), \tag{2.21}$$

where marginal probability at time t, $p_{i,t}(\sigma)$, is obtained from $p_t(\boldsymbol{\sigma})$ as

$$p_{i,t}(\sigma) = \sum_{\boldsymbol{\sigma}\setminus\sigma_i} p_t(\boldsymbol{\sigma}). \tag{2.22}$$

The object $p_{i,t}(\sigma)$ denotes the probability of observing the state σ at node i and time t. The symbol $\sum_{\boldsymbol{\sigma}\setminus\sigma_i}$ denotes summation over all spins except for σ_i.

Up to now, we have not specified the explicit form of the coupling strenght J_{ij} in the local fields definition, equation (2.5), responsible for the introduction of disorder in the

system. The most common type of disorder regards the nature of the pairwise interactions, achieved by introducing some kind of randomness to J_{ij}. For instance, we may choose each J_{ij} randomly from a gaussian distribution, promoting the coexistence of ferromagnetic ($J_{ij} > 0$) and anti-ferromagnetic ($J_{ij} < 0$) interactions in the system, in contrast to the exclusively ferromagnetic scenario promoted by choosing $J_{ij} = J > 0$ for all pairs, where J is a constant.

Another kind of disorder, called topological disorder, regards the structure of the underlying complex network. On its pioneering work [25], Ising presented the analytical solution of the ferromagnetic one dimensional chain with nearest neighbour interactions in the absence of external fields, featuring no phase transition. Later, in 1944, Lars Onsager presented the solution for the two dimensional ferromagnetic nearest neighbour lattice, or square lattice, that undergoes a continuous phase transition at $T > 0$ in the absence of external fields [30]. These two equilibrium statistical mechanics examples show the importance of the lattice structure for phase transitions, while the development of network science emphasizes the central role of network heterogeneities on dynamical processes in general [46].

Topological disorder can be introduced in the system if we identify each spin to a node of a random graph represented by the adjacency matrix $\boldsymbol{C}$, that encodes the structure of the underlying complex network through its elements as

$$C_{ij} = \begin{cases} 1, \text{ if the pair of spins } (i,j) \text{ is connected,} \\ 0, \text{ otherwise.} \end{cases} \tag{2.23}$$

The complex network is incorporated in the model through a simple modification of the local fields, namely

$$h_i(\boldsymbol{\sigma}_t) = \sum_{j=1}^{N} J_{ij} C_{ij} \sigma_{j,t} = \sum_{j \in \partial_i} J_{ij} \sigma_{j,t}. \tag{2.24}$$

The neighbourhood of the ith spin, represented by ∂_i, is the set of indexes j such that $C_{ij} = 1$ and it represents the spins that are coupled to σ_i. The number of connections of a spin, called the coordination number or degree of the spin i, is defined as

$$K_i = \sum_{j=1}^{N} C_{ij}. \tag{2.25}$$

The vector $\boldsymbol{K} = (K_1, \cdots, K_N)$ contains the degrees of all spins, and its entries are independent random variables drawn from the distribution

$$p_k = \lim_{N \to \infty} \frac{1}{N} \sum_{i=1}^{N} \delta_{K_i,k}. \tag{2.26}$$

The distribution p_k is an input of the network model. The mean degree c and the variance

δ^2 of p_k are given by

$$c = \sum_{k\geq 0} k p_k, \tag{2.27}$$

$$\delta^2 = \sum_{k\geq 0} k^2 p_k - c^2. \tag{2.28}$$

The literature concerning fully connected systems, *i.e.*, networks where each spin is connected to all others is vast and the phenomenology of such systems is well known. Important examples, both in and out of equilibrium, are the fully connected ferromagnet, or Curie-Weiss model [47] and fully connected gaussian couplings model, Sherrington-Kirkpatrick spin glass [28, 40]. However, real networks present finite connectivity and degree fluctuations, since the number of connections per spin changes along the network. Therefore, the description of real dynamical processes on top of complex networks should include such features. In this work we address the impact of degree fluctuation, developing a theory that retains the effect of the network structure and whose non-equilibrium dynamics can be solved exactly. We consider ferromagnetic coupling strenghts because of their simplicity, and by doing so, disorder is introduced in the system only through the degrees K_i. Hence, the local field in our model is given by

$$h_i(\boldsymbol{\sigma}_t) = \frac{J}{c} \sum_{j\in\partial_i} \sigma_{j,t}, \tag{2.29}$$

where the scaling with the mean degree c ensures extensivity, when $c \to \infty$, for the system's Lyapunov function [45]

$$L(\boldsymbol{\sigma}_t) = -\sum_{i=1}^{N} |h_i(\boldsymbol{\sigma}_t)|\sigma_i, \tag{2.30}$$

once the summation in equation (2.29) is of $\mathcal{O}(c)$. A Lyapunov function is a monotonically decreasing function that is bounded from below, and which recovers the pseudohamiltonian

$$H(\boldsymbol{\sigma}) = -\frac{J}{c} \sum_{i=1}^{N} \sum_{j\in\partial_i} \sigma_j \sigma_i \tag{2.31}$$

once the system reached its stationary configuration $\boldsymbol{\sigma}$. In addition, we consider simple undirected networks, where the interaction between two spins is symmetric and without self-loops ($C_{ii} = 0$ for any i), also called simple undirected networks [14].

Having set up the model, we now proceed to the derivation of the dynamical equations. From the Markov process (2.15), the marginalization in equation (2.22) becomes

$$p_{i,t+1}(\sigma) = \sum_{\boldsymbol{\sigma}'} p_t(\boldsymbol{\sigma}') \frac{1}{2}\{1 + \sigma_i \mathcal{F}[h_i(\boldsymbol{\sigma}')]\}, \tag{2.32}$$

yielding for the local magnetization (2.21)

$$m_{i,t+1} = \sum_{\boldsymbol{\sigma}'} p_t(\boldsymbol{\sigma}') \mathcal{F}\left[h_i(\boldsymbol{\sigma}')\right]. \tag{2.33}$$

Considering the explicit form of the local field in equation (2.29), we can write

$$h_i(\boldsymbol{\sigma}') = \frac{JK_i}{c}\left(\frac{1}{K_i}\sum_{j\in\partial_i}\sigma_j\right), \tag{2.34}$$

where the term in parentesis is the magnetization of the neighbourhood ∂_i. Considering that the random variables $\sigma_j \in \partial_i$ are drawn from a probability distribution $P_t(\sigma)$, from the law of the large numbers, the convergence

$$\frac{1}{K_i}\sum_{j\in\partial_i}\sigma_{j,t} \to u_t \tag{2.35}$$

is established as $c \to \infty$, where u_t is the average of the probability $P_t(\sigma)$

$$u_t = \sum_{\sigma}\sigma P_t(\sigma). \tag{2.36}$$

Consequently, the local field converges to the heterogeneous mean field

$$h_i(\boldsymbol{\sigma}'_t) \to \frac{JK_iu_t}{c}. \tag{2.37}$$

We call it heterogeneous mean field because it includes the local fluctuations in the network structure through the degree K_i. The probability $P_t(\sigma)$ of observing a state σ on the neighbourhood of an arbitrary spin ∂_i is equal to the probability of randomly selecting an edge with a state σ at one of its ends, therefore

$$P_t(\sigma) = \frac{\sum_{i,j=1}^{N} C_{ij}\sum_{\sigma} p_{i,t}(\sigma')\delta_{\sigma',\sigma}}{\sum_{i,j=1}^{N} C_{ij}}. \tag{2.38}$$

Due to equation (2.37), the local fields become independent of $\boldsymbol{\sigma}'$, rendering a trivial summation in equation (2.33), resulting in

$$m_{i,t+1} = \mathcal{F}\left(\frac{\beta JK_iu_t}{c}\right). \tag{2.39}$$

This equation allows to study the dynamics of the local magnetization. By means of the substitution of this last result in equation (2.20), we obtain the global magnetization

$$m_{t+1} = \lim_{N\to\infty}\frac{1}{N}\sum_{i=1}^{N}\mathcal{F}\left(\frac{\beta JK_iu_t}{c}\right), \tag{2.40}$$

which can be written explicitly in terms of the distribution p_k, equation (2.26), by introducing a Kronecker's delta on the degrees as

$$m_{t+1} = \sum_{k\geq 0}\left(\lim_{N\to\infty}\frac{1}{N}\sum_{i=1}^{N}\delta_{K_i,k}\right)\mathcal{F}\left(\frac{\beta Jku_t}{c}\right) = \sum_{k\geq 0}p_k\mathcal{F}\left(\frac{\beta Jku_t}{c}\right). \tag{2.41}$$

By taking the limit of infinite c in the equation for the global magnetization, we get

$$m_{t+1} = \int_0^{\infty} dg\nu(g)\mathcal{F}\left(\beta Jgu_t\right), \tag{2.42}$$

where $\nu(g)$ is the rescaled degree distribution

$$\nu(g) = \lim_{c\to\infty} \sum_{k\geq 0} p_k \delta\left(g - \frac{k}{c}\right). \tag{2.43}$$

This result shows that the dynamical evolution of the magnetization is conditioned to the evolution of the unknown parameter u_t. Combining equations (2.36) and (2.38) and performing the summation over j, we obtain

$$u_t = \frac{\sum_i K_i m_{i,t}}{\sum_i K_i}, \tag{2.44}$$

which represents the spatial average of the local magnetizations $m_{i,t}$ weighted by the degrees K_i. In the thermodynamic limit $N \to \infty$, we use equation (2.39) to write u_{t+1} as

$$u_{t+1} = \frac{1}{c} \sum_{k\geq 0} k p_k \mathcal{F}\left(\frac{\beta J k u_t}{c}\right), \tag{2.45}$$

and finally take the limit $c \to \infty$ to obtain

$$u_{t+1} = \int_0^\infty dg \nu(g) g \mathcal{F}(\beta J g u_t). \tag{2.46}$$

Equations (2.42) and (2.46) define a closed set of recurrence relations for the dynamical behavior of the global magnetization. Note that the order of the limits is important. By taking first the limit $N \to \infty$ and then $c \to \infty$, we ensure that $c/N \to 0$, allowing the rescaled degrees $G_i = K_i/c$ to fluctuate around the mean value c. This procedure corresponds to the scaling $c \propto N^a$, with $0 \leq a < 1$ and this regime defines what we call the high connectivity limit [36]. The high connectivity limit lies somehow between the fully connected case ($c \propto N$) and the sparse case (finite c). In Appendix A, we present an alternative derivation of this mean field dynamical set of equations based on the generating functional formalism [40, 48], a more rigorous and exact method.

Equation (2.39) allows us to derive an equation for the full distribution of local magnetizations. Even though the macroscopic magnetization m_t defines a single path through phase space, each spin on the heterogeneous network displays a local magnetization that fluctuates around this global value. The probability distribution $\mathcal{P}_t(m)$ of local magnetizations at time t can be determined straightforwardly from the high connectivity limit of equation (2.39), namely

$$m_{i,t+1} = \mathcal{F}(J\beta G_i u_t), \tag{2.47}$$

with $G_i \sim \nu(g)$. We see that $m_{i,t+1}$ is a function of the random variable G_i, and therefore it is a random variable itself. Since we know the distribution $\nu(g)$ og G_i in the high connectivity limit, we can use the method of change of variables, presented in Appendix B, and obtain a general equation for the full distribution of local magnetizations

$$\mathcal{P}_t(m) = \frac{T}{J u_t} \left| \frac{d}{dm} \mathcal{F}^{-1}(m) \right| \nu\left[\frac{T\mathcal{F}^{-1}(m)}{J u_t}\right], \tag{2.48}$$

which is determined by the explicit choices of the distributions $\nu(g)$ and $\mu(\zeta)$. The quantity $\mathcal{F}^{-1}$ is the inverse of the activation function $\mathcal{F}$. The first moment of $\mathcal{P}_t(m)$ gives again the global magnetization

$$m_t = \int_0^1 dm' \, \mathcal{P}_t(m'). \tag{2.49}$$

Equations (2.15), (2.42), (2.46) and (2.48) are the central results of this work, allowing to determine the macroscopic evolution of the system, as well as to characterize microstate probabilities and fluctuations of local magnetizations.

Having introduced the rescaled degree distribution $\nu(g)$, equation (2.43), we can define more precisely what an heterogeneous network is in terms of its relative variance

$$\lim_{c\to\infty} \frac{\delta^2}{c^2} \equiv \Delta^2, \tag{2.50}$$

which quantifies the degree fluctuations. A graph is called homogeneous if $\Delta^2 = 0$, and heterogeneous if $\Delta^2 > 0$. Even though homogeneous graphs can display degree fluctuations for finite N and c, such fluctuations are irrelevant in the high connectivity limit because their rescaled distribution $\nu(g)$ becomes peaked at the mean value $g = 1$ (which implies $\Delta^2 = 0$). Important examples of homogeneous ensembles are the Erdős-Rényi and the regular random graphs [15]. Heterogeneous graphs, on the other hand, are those that display degree fluctuations that are "strong enough" in comparison to c to remain important in the high connectivity limit, giving rise to finite rescaled variance Δ^2. This distinction between heterogeneous and homogeneous complex networks leads to an important feature of the model. For those degree distributions such that $\Delta^2 = 0$, we obtain $\nu(g) = \delta(g - 1)$, since $K_i = c$ for any i, reducing the dynamical equations (2.42) and (2.46) to a single recurrence relation

$$m_{t+1} = \mathcal{F}(\beta J m_t). \tag{2.51}$$

This is the result for fully connected models, but interestingly $\Delta^2 = 0$ is not a feature exclusive to such trivial configuration. The Erdős-Rényi ensemble of random graphs [15] is an example in which p_k presents fluctuations, but $\nu(g)$ has a vanishing relative variance (as shown in Appendix C). Therefore, equation (2.51) shows that networks with weak or no degree fluctuations behave like fully connected ones, establishing the latter as an universality class for homogeneous systems.

We finish this section with a discussion about the generation of random graphs from a given degree sequence $\boldsymbol{K}$, called configuration models [14], and present a useful approximation for their adjacency matrix in the high connectivity limit that will come in hand for the simulation results presented in Chapter 3. The simplest algorithm to generate random graphs from the configuration model is the pairing model [49]. First, a set of nodes is generated, each with K_i connections to perform; then, pairs of nodes are uniformly chosen and connected. When a pair is connected twice or a loop is generated (a node connected to itself), this graph is neglected and the process is restarted. As N grows, this

algorithm becomes very slow and inefficient, since lots of trials are neglected, rendering numerical simulations of large systems very difficult. To obtain an approximation to avoid the necessity of using sophisticated algorithms to simulate the model, we start by noting that, through substitution of equation (2.44) in equation (2.37), we can write the local field as

$$h_i(\boldsymbol{\sigma}_t) = \frac{J}{Nc} \frac{\sum_{j=1}^{N} K_i K_j m_{j,t}}{\left(\frac{1}{N}\sum_{j=1}^{N} K_j\right)}. \tag{2.52}$$

As N grows, $\frac{1}{N}\sum_{j=1}^{N} K_j \to c$, and then taking the limit $c \to \infty$ with the rescaling $G_i = K_i/c$, we have

$$h_i(\boldsymbol{\sigma}_t) \to \frac{J}{N} \sum_{j=1}^{N} G_i G_j m_{j,t}. \tag{2.53}$$

By comparing equation (2.53) with the local field

$$h_i(\boldsymbol{\sigma}_t) = \frac{J}{c} \sum_{j=1}^{N} C_{ij} \sigma_{j,t}, \tag{2.54}$$

we see that the entries of the adjacency matrix $\boldsymbol{C}$ may be replaced, in the high connectivity limit, by

$$C_{ij} = \frac{c}{N} G_i G_j (1 - \delta_{i,j}). \tag{2.55}$$

In Chapter 3 we confirm the equivalence between the configuration model and the fully connected network defined by the adjacency matrix with elements given by (2.55) through numerical simulations. Even though a fully connected network is more expensive in terms of computational memory, simulations are more efficient than the trial and error generation process of the pairing algorithm.

2.3 Critical exponents of the Ising model

We end this chapter by discussing the concept of critical exponents. Statistical mechanics is concerned with providing a microscopic description of macroscopic thermodynamic phenomena, and one of its biggest triumphs is the understanding of phase transitions and critical phenomena [21], both stationary and dynamical [50].

For magnetic systems such as the Ising model, critical phenomena may be described in terms of the magnetization m_t. The transition between the ordered and the disordered phase is defined in terms of the stationary value $m = \lim_{t\to\infty} m_t$. If $m > 0$, a macroscopic fraction of the spins is aligned and the system is in an ordered ferromagnetic phase, while for $m = 0$ the system is in a disordered paramagnetic phase. In this section, we present a brief survey of the critical behavior of the magnetization in the fully connected Ising model [7]. We focus on the dynamical critical exponent for the relaxation of m_t to the stationary value m, and on the stationaty critical exponent for the dependence of the value m on the rescaled temperature $\frac{T_c - T}{T_c}$.

Given a ferromagnetic initial state $T < T_c$ with very small magnetization, after an abrupt change $T \to T_c$ on the temperature of the system, it will relax towards the new stationary magnetization. After a transient short time regime, sensitive to initial conditions, the long time relaxation of m_t behaves as a power law [51]

$$m_t \propto t^{-z_1}, \quad (t \gg 1), \tag{2.56}$$

where $m_0 > 0$ is the initial magnetization and $m = 0$. Considering a fully connected network and the hyperbolic tangent activation function $\mathcal{F}(x) = \tanh(x)$, we recover the Curie-Weiss model [52], whose dynamics is given by (2.51)

$$m_{t+1} = \tanh(\beta J m_t). \tag{2.57}$$

The iteration of this equation for long times shows that the magnetization has a power law decay with $z_1 = 1/2$. This value for the dynamical critical exponent defines a universality class for systems with purely dissipative dynamics without a conserved order parameter, known as "model A" [53].

The stationary critical exponent λ is defined as the leading term of the Taylor expansion in terms of $\frac{T_c - T}{T_c}$ around zero,

$$m \propto \left(\frac{T_c - T}{T_c}\right)^{\lambda_1}. \tag{2.58}$$

Setting $m_t = m$ in equation (2.57), the stationary transcendental equation for the magnetization of the Curie-Weiss model is obtained as

$$m = \tanh(\beta J m). \tag{2.59}$$

By expanding the hyperbolic tangent in a Taylor series in $\frac{T_c - T}{T_c}$ around zero we find that the leading order term for $T \to T_c$ is

$$m = \sqrt{3}\left(\frac{T_c - T}{T_c}\right)^{\frac{1}{2}}, \tag{2.60}$$

so $\lambda_1 = 1/2$. This is the value for the usual homogeneous mean-field description of Ising models, and also define a universality class.

Finally, an interesting relation between the correlation length ξ, a purely stationary quantity, and the relaxation time τ, a purely dynamical quantity. For a temperature $T \neq T_c$, the system relaxes exponentially fast to the stationary in the form

$$m_t \propto e^{-\frac{t}{\tau}}. \tag{2.61}$$

The relation between τ and ξ is described in terms of the dynamical Z exponent as [54]

$$\tau \propto \xi^Z. \tag{2.62}$$

Since the correlation length of the Curie-Weiss model diverges as $T \to T_c$ from the ferromagnetic phase like $\xi \propto |T_c - T|^{-1/2}$ and the relaxation time as $\tau \propto |T_c - T|^{-1}$, we have $Z = 2$.

In Chapter 3, we investigate the effect of degree fluctuation and noise thresholds in the general behavior of the system and obtain the critical exponents z_1, λ_1 and Z for the heterogeneous and arbitrary threshold noise Ising model, as well as their counterparts for the variance of the local magnetization distribution $\mathcal{P}(m)$.

3 Results and discussion

In the previous chapter we presented the derivation of the fundamental equations that describe the dynamical behavior of the Ising model on highly connected random graphs. These equations are valid for generic degree and threshold noise distributions. In this chapter, we explore in detail the consequences of such equations by choosing specific forms for the distributions p_k and $\mu(\zeta)$.

Considering the degree distribution, we choose the negative binomial distribution

$$p_k = \frac{\Gamma(\alpha + k)}{k!\Gamma(\alpha)} \left(\frac{c}{\alpha}\right)^k \left(\frac{\alpha}{\alpha + c}\right)^{\alpha+k}, \tag{3.1}$$

whose variance is given by

$$\delta^2 = \frac{c^2}{\alpha} + c. \tag{3.2}$$

Here, c is the mean degree and $\alpha > 0$ is a parameter that controls δ^2. The associated rescaled degree distribution, also calculated in Appendix C, is given by

$$\nu(g) = \frac{\alpha^\alpha}{\Gamma(\alpha)} g^{\alpha-1} e^{-\alpha g}, \tag{3.3}$$

where the variance of $\nu(g)$ reads

$$\Delta^2 = \frac{1}{\alpha}. \tag{3.4}$$

We note that this is an interesting degree distribution because it allows to interpolate between homogeneous graphs ($\alpha \to \infty$ and $\Delta^2 \to 0$) and heterogeneous graphs ($\alpha \to 0$ and $\Delta^2 \to \infty$) by changing a sigle parameter.

We consider two distributions of threshold noise, namely

$$\mu_h(\zeta) = \frac{1}{2}[1 - \tanh^2(\zeta)], \tag{3.5}$$

$$\mu_\kappa(\zeta) = \frac{1}{2}(1 + \zeta^{2\kappa})^{-\left(1+\frac{1}{2\kappa}\right)}, \tag{3.6}$$

with integer κ. A plot of each of these distributions as functions of ζ is presented in figure 3.0.1. The associated activation functions are given by

$$\mathcal{F}_h(x) = \tanh(x), \tag{3.7}$$

$$\mathcal{F}_\kappa(x) = \frac{1}{2} x (1 + x^{2\kappa})^{-\frac{1}{2\kappa}}. \tag{3.8}$$

The first reason for these choices is related to the tail of such distributions. As shown in the left panel of figure 3.0.1, the hyperbolic tangent distribution μ_h, equation (3.5), has an exponential tail, while the algebraic distribution μ_κ, equation (3.6), decays as a power law $|\zeta|^{-2\kappa-1}$ for $|\zeta| \gg 1$, presenting a slower tail that increases the probability of stronger thermal fluctuations. Therefore these distributions allow to explore different heat baths.

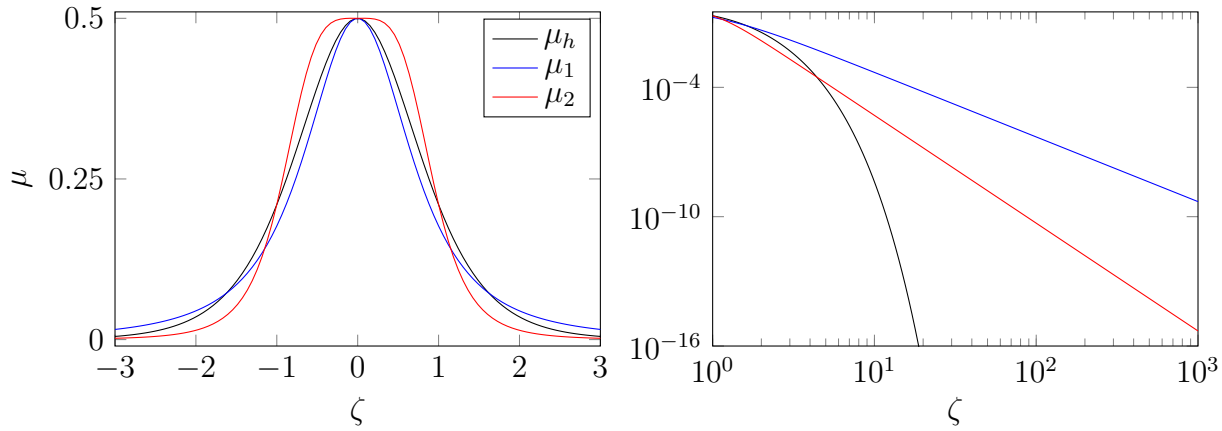

Figure 3.0.1 – Noise distributions, equations (3.5) and (3.6). The left panel presents the hyperbolic and algebraic, with $\kappa = 1$ and $\kappa = 2$, distributions as a function of ζ. The right panel presents a log-log plot showing the power law decaying of the algebraic distributions for the same values of the index κ. On the inset, we pshow a semilog plot showing the exponential decaying of the hyperbolic distribution.

The second reason has to do with the stationary solution of equation (2.15) for the microstate probability, as mentioned in Section 2.2. From the heterogeneous mean field approximation, equation (2.37), we see that the local fields in the high connectivity limit become independent of the configuration $\boldsymbol{\sigma}'$, allowing to directly perform the summation over states to obtain

$$p_{t+1}(\boldsymbol{\sigma}) = \prod_{i=1}^{N} \frac{1}{2}[1 + \sigma_{i,t+1}\mathcal{F}\left(J\beta G_i u_t\right)]. \tag{3.9}$$

Setting $u_t = u$ in the last result, we obtain the fixed point value of the microstate probability

$$p(\boldsymbol{\sigma}) = \prod_{i=1}^{N} \frac{1}{2}[1 + \sigma_i\mathcal{F}\left(J\beta G_i u\right)]. \tag{3.10}$$

By choosing the hyperbolic tangent threshold noise distribution $\mu_h(\zeta)$, which corresponds to the original formulation of the dynamics of Ising spins presented by Glauber [39], equation (3.9) assumes the form of a Boltzmann distribution, which is a consequence of detailed balance and thermodynamic equilibrium [45]. From equation (2.19) for the stationary microstate probability, duplicating the configuration space by introducing a new set of Ising variables $\lambda_i = \pm 1$ and using equation (2.29) for the local fields, we can rewrite the probability distribution as

$$p(\boldsymbol{\sigma}) = \frac{1}{Z}\prod_{i=1}^{N}\sum_{\boldsymbol{\lambda}} e^{\frac{\beta J}{c}\sum_{i,j=1}^{N} C_{ij}\lambda_i\sigma_j}, \tag{3.11}$$

where the notation $\sum_{\boldsymbol{\lambda}}$ denotes sum over all 2^N possible configurations of the vector $\boldsymbol{\lambda}$. Since $\sum_i C_{ij}\lambda_i = \sum_{i\in\partial_j} \to K_i u$ for large c, and using the explicit form of the normalization

factor, we obtain

$$p(\boldsymbol{\sigma}) = \frac{\prod_{i=1}^{N} e^{\beta J G_i \sigma_i u}}{\prod_{i=1}^{N} \cosh(\beta J G_i u)}. \tag{3.12}$$

From the identity

$$e^{\beta J G_i \sigma_i u} = \frac{1}{2}[\cosh(\beta J G_i u) + \sigma_i \sinh(\beta J G_i u)], \tag{3.13}$$

we finally recover equation (3.10) for $\mathcal{F}_h$, namely

$$p(\boldsymbol{\sigma}) = \prod_{i=1}^{N} \frac{1}{2}[1 + \sigma_i \tanh(J\beta G_i u)]. \tag{3.14}$$

However, note that the stationary form of the microstate probability is not generally Boltzmann-like. In fact, this happens for the majority of noise thresholds, strongly indicating the breakage of detailed balance. To explore the consequences of that, we consider the algebraic threshold noise $\mu_\kappa(\zeta)$.

In the rest of this chapter, we present results for the stationary and the dynamical behaviour. The main results are the critical exponents for the global magnetization and for the variance of the distribution of local magnetizations in both regimes.

3.1 Stationary behaviour

The fixed point solutions of the dynamical equations (2.42) and (2.46) are obtained as $t \to \infty$ by setting $u_t = u$

$$m = \int_0^\infty dg \nu(g) \mathcal{F}(\beta J g u), \tag{3.15}$$

$$u = \int_0^\infty dg \nu(g) g \mathcal{F}(\beta J g u). \tag{3.16}$$

These equations generalize those presented in [36], derived through equilibrium methods [29], and they reduce to the Curie-Weiss mean field equation [47] in the homogeneous limit $\alpha \to \infty$ for $\mathcal{F}_h(x)$ (see equation (3.7)). This result reveals another aspect of the present work, namely the fact that through the dynamical set of equations (3.15) and (3.16), obtained in the previous chapter, one can analyze stationary states of systems that do not evolve to thermodynamic equilibrium, which is expected to happen for the majority of the distributions of threshold noise.

The fixed-point equations (3.15) and (3.16) admit a trivial solution $u = m = 0$, associated to a paramagnetic phase, and by means of the property $\mathcal{F}(0) = 0$, a series expansion of the self-consistent equation for u up to first-order shows that a nontrivial solution $|u| > 0$ arises below the critical temperature

$$T_c = \left.\frac{d\mathcal{F}(x)}{dx}\right|_{x=0} J(1 + \Delta^2), \tag{3.17}$$

with $x = \beta J g u$. In the last result, we made use of the fact that

$$\langle G \rangle = \frac{\alpha^\alpha}{\Gamma(\alpha)} \int_0^\infty dg g^\alpha e^{-\alpha g} = 1, \tag{3.18}$$

vide integral 3.351.2 of Gradstheyn and Rhyzik's table of Integrals, Series and Products [55]. A first interesting characteristic of equation (3.17) is that the tail of the noise threshold is irrelevant for the critical temperature, since equation (3.18) only depends on the behavior of $\mathcal{F}(x)$ near $x = 0$. Besides that, T_c is finite for finite Δ^2, but it diverges in the heterogeneous limit $\Delta^2 \to \infty$, in accordance to [34, 35]. In such case, the system lies in a ferromagnetic phase $|m| > 0$ for any value of temperature, a feature exclusive to networks with a infinite number of nodes [33]. In the homogeneous limit $\Delta^2 \to 0$, equation (3.17) recovers the Curie-Weiss critical temperature, multiplied by a constant factor given by the derivative of the activation function at zero. Since in our cases both choices of $\mathcal{F}$ give $\frac{d\mathcal{F}}{dx} = 1$, they yield the same critical temperature

$$T_c = J(1 + \Delta^2). \tag{3.19}$$

The phase diagram of the model in the case of a negative binomial degree distribution is presented in figure 3.1.1. The magnetization profile of equation (2.42) as a function of

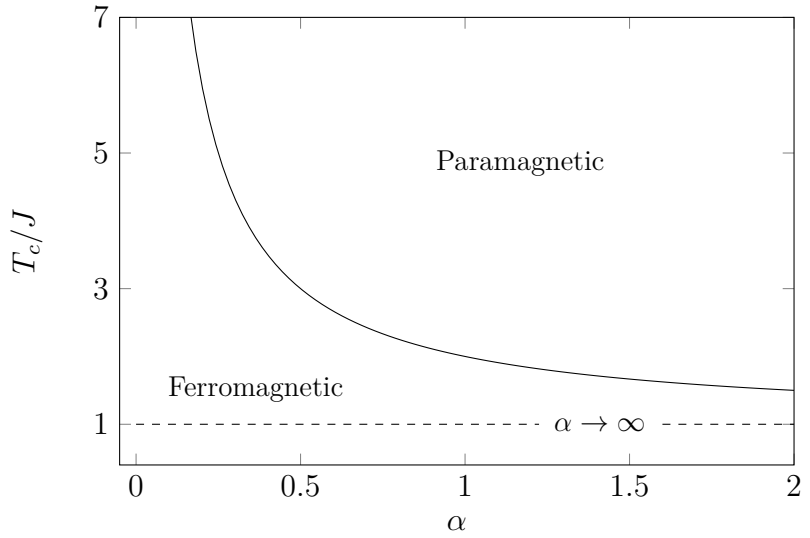

Figure 3.1.1 – Phase diagram for the Ising model on heterogeneous networks in the high connectivity limit. The rescaled degree distribution is given by equation (3.3), with relative variance $\Delta^2 = \frac{1}{\alpha}$. The black solid line represents a continuous phase transition between ferromagnetic and paramagnetic phases, while the dashed line represents the fully connected critical temperature, that meets the solid line at infinity.

temperature is presented in figure 3.1.2, showing that the system undergoes a continuous phase transition between a ferromagnetic phase ($|m| > 0$) and a paramagnetic phase ($|m| = 0$) at the critical temperature T_c given by equation (3.19). Once again, the resullts for the fully connected Ising model arises in the asymptotic limit $\alpha \to \infty$.

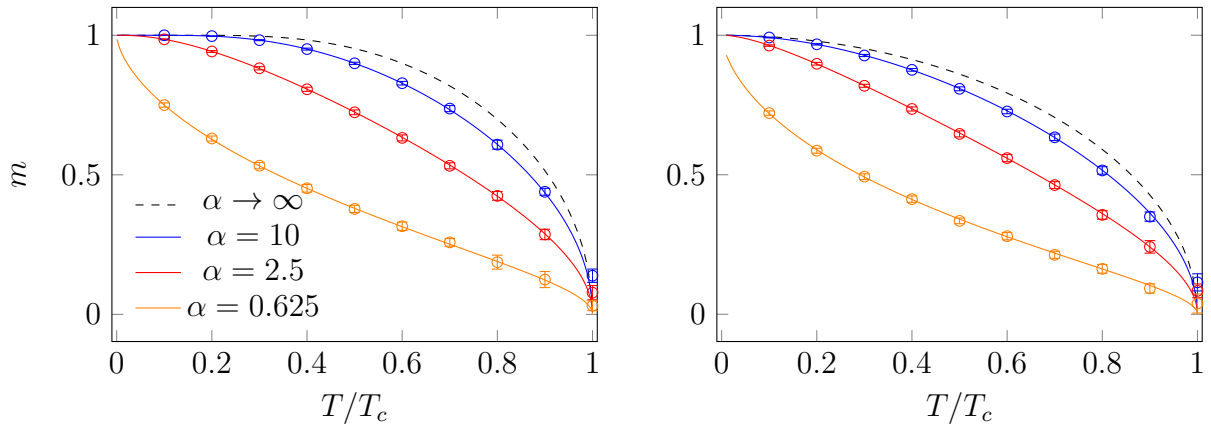

Figure 3.1.2 – Magnetization profile in terms of temperature for μ_h, equation (3.5) in the left and μ_κ with $\kappa = 1$, equation (3.6), in the right. The parameter α determines the relative variance $\Delta^2 = \frac{1}{\alpha}$. Solid lines are obtained from the solution of equations (3.15) and (3.16), while circles denote results obtained through Monte-Carlo simulations with $N = 10^4$ and $c = 10^2$. The standard deviation, given by the vertical bars, is obtained through average over 10 independent simulations on random graphs generated by equation (2.55).

The fixed-point value of u also determines the stationary distribution of local magnetizations (2.48)

$$\mathcal{P}(m) = \frac{T}{Jgu}\left|\frac{d}{dm}\mathcal{F}^{-1}(m)\right|\nu\left[\frac{T\mathcal{F}^{-1}(m)}{Ju}\right], \tag{3.20}$$

whose support for $u > 0$ ($u < 0$) is the interval $m \in [0, 1]$ ($m \in [-1, 0]$). From the inverse activation function $\mathcal{F}^{-1}(ax)$ for each case, given by

$$\mathcal{F}_h^{-1}(ax) = \frac{\operatorname{atanh}(x)}{a}, \tag{3.21}$$

$$\mathcal{F}_\kappa^{-1}(ax) = \frac{x}{a(1-x)^{\frac{1}{2\kappa}}}, \tag{3.22}$$

the explicit stationary forms $\mathcal{P}(m)$ for each of the noise distributions $\mu(\zeta)$ is obtained from equations (3.5) and (3.6)

$$\mathcal{P}_h(m) = \frac{\alpha^\alpha}{\Gamma(\alpha)}\frac{T}{J|u|(1-m^2)}\left[\frac{\operatorname{atanh}(m)}{\beta Ju}\right]^{\alpha-1} e^{-\frac{T\alpha\operatorname{atanh}(m)}{Ju}}, \tag{3.23}$$

$$\mathcal{P}_\kappa(m) = \frac{\alpha^\alpha}{\Gamma(\alpha)}\frac{T}{J|u|(1-m^{2\kappa})^{1+\frac{1}{2\kappa}}}\left[\frac{m}{\beta Ju(1-m^{2\kappa})^{\frac{1}{2\kappa}}}\right]^{\alpha-1} e^{-\frac{T\alpha m}{Ju(1-m^{2\kappa})^{\frac{1}{2\kappa}}}}, \tag{3.24}$$

where $\mathcal{P}_h$ is the result for the hyperbolic threshold noise distriibution μ_h, while $\mathcal{P}_k$ for the algebraic threshold noise distribution μ_κ. Interestingly, the behavior for small m of both distributions (3.23) and (3.24) is

$$\mathcal{P}_{h,\kappa}(m) \simeq \frac{\alpha^\alpha}{\Gamma(\alpha)}\frac{T}{J|u|}\left(\frac{Tm}{Ju}\right)^{\alpha-1}. \tag{3.25}$$

Thus, $\mathcal{P}(m)$ has a power law divergence for $m \to 0$ when $\alpha < 1$, similarly to what is observed in other spin models on random graphs [36]. This property reflects the singular

behavior of $\nu(g)$ at $g = 0$ for $\alpha < 1$. For $\alpha \geq 1$, $\mathcal{P}(m)$ converges to a finite value as $m \to 0$. Panels (a) and (b) of figure 3.1.3 illustrate $\mathcal{P}(m)$ as a function of m for $\alpha = 2.5$. The variance of $\mathcal{P}(m)$, $\mathrm{Var}(m)$, as a function of the temperature T for different values of α is presented in panels (c) and (d) of figure 3.1.3. The variance is calculated from the expression

$$\mathrm{Var}(m) = \int_0^\infty dg\nu(g)\mathcal{F}^2\left(\frac{Jgu}{T}\right) - \left[\int_0^\infty dg\nu(g)\mathcal{F}\left(\frac{Jgu}{T}\right)\right]^2. \tag{3.26}$$

The variance $\mathrm{Var}(m)$ goes to zero for $T \to 0$ and $T \to T_c$, which implies that the distribution $\mathcal{P}(m)$ becomes peaked for $m = 0$ and $m = 1$, while for intermediate values of temperature the variance is finite. In addition, $\mathrm{Var}(m)$ vanishes as α increases, showing that degree fluctuations induce fluctuations in the local magnetizations. Also, due to the interplay between heterogeneity and temperature effects, $\mathrm{Var}(m)$ presents a non monotonic dependence on T, with a maximum at a certain value of temperature that depends on α.

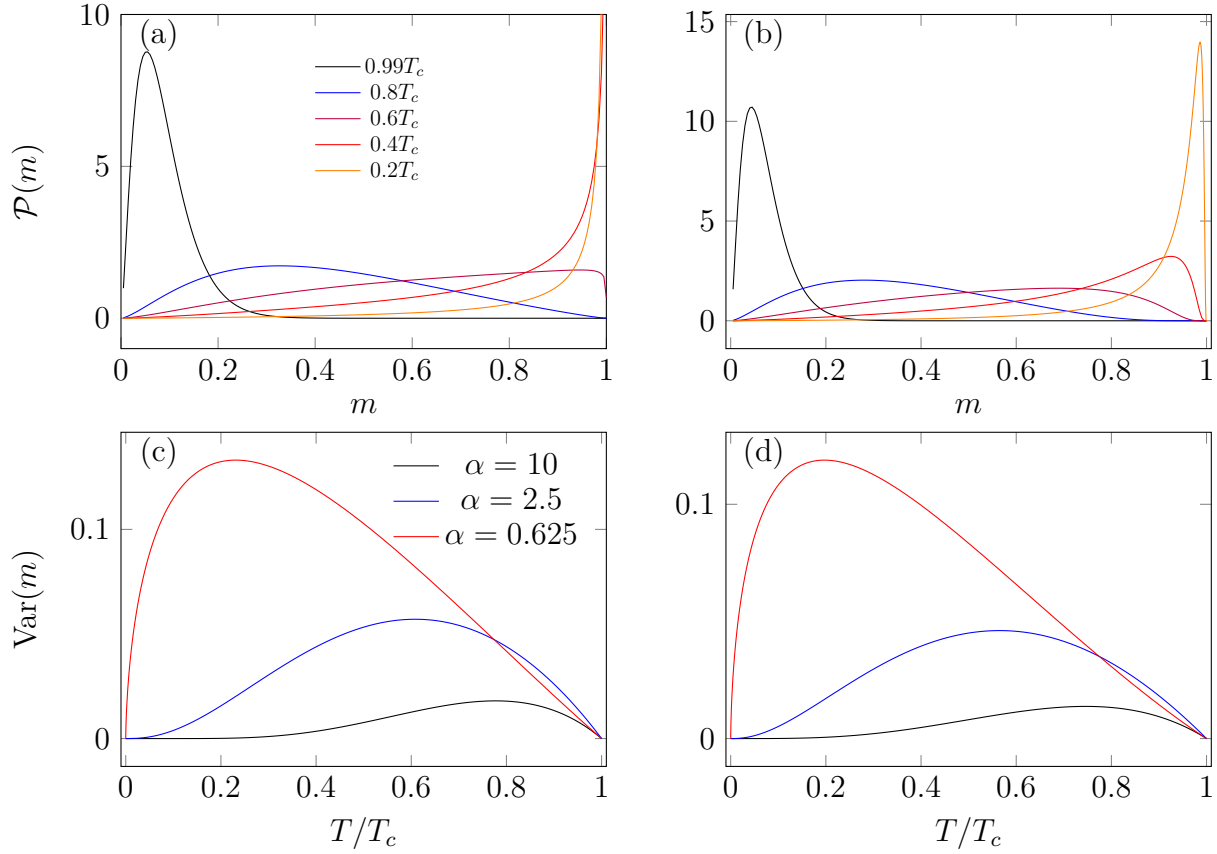

Figure 3.1.3 – Top row: distribution of local magnetizations for different values of temperature (in fractions of T_c) for μ_h (a) and μ_1 (b) with $\alpha = 2.5$, obtained through equations (3.23) and (3.24). Bottom row: $\mathrm{Var}(m)$ as a function of temperature for μ_h (c), equation (3.5) and μ_1 (d), equation (3.6), obtained through equation (3.26), for different values of the parameter α. The variance of the rescaled degree distribution is given by $\Delta^2 = \frac{1}{\alpha}$.

In the sequel, we compute the critical exponents that characterize the mean and the variance of $\mathcal{P}(m)$. By approximating T_c from the ferromagnetic phase, m and $\mathrm{Var}(m)$ vanish as

$$m \propto \left(\frac{T_c - T}{T_c}\right)^{\lambda_1}, \tag{3.27}$$

$$\mathrm{Var}(m) \propto \left(\frac{T_c - T}{T_c}\right)^{\lambda_2}. \tag{3.28}$$

As shown in Appendix D, by expanding equations (2.42) and (2.46) for the hyperbolic tangent threshold noise μ_h, we obtain

$$m_h \simeq \pm\sqrt{\frac{3\langle G^2\rangle}{\langle G^4\rangle}}\left(\frac{T_c - T}{T_c}\right)^{\frac{1}{2}}, \tag{3.29}$$

$$\mathrm{Var}(m)_h \simeq \pm\frac{3\langle G^2\rangle}{\langle G^4\rangle}(\langle G^2\rangle - 1)\left(\frac{T_c - T}{T_c}\right), \tag{3.30}$$

where $\langle G^n\rangle$ denotes the nth moment of the rescaled degree distribution $\nu(g)$, given by

$$\langle G^n\rangle = \int_0^\infty dg g^n \nu(g). \tag{3.31}$$

The critical exponent for the average magnetization m_h, $\lambda_1 = 1/2$, is in accordance with previous results [34, 35] for degree distributions with finite $\langle G^4\rangle$, exhibiting the usual mean field critical value of equation (2.60) in Section 2.3. The variance vanishes linearly as $T \to T_c$, $\lambda_2 = 1$, exactly like the variance of the effective field distribution in the replica symmetric solution of the Sherrington-Kirkpatrick model [28].

For the algebraic noise threshold, the series expansion in powers of u contains divergent terms so it must be done in powers of $u^{2\kappa}$. This change of variables, also presented in Appendix D, leads to the expressions

$$m_\kappa \simeq \pm\left(\frac{2\kappa\langle G^2\rangle}{\langle G^{2+2\kappa}\rangle}\right)^{\frac{1}{2\kappa}}\left(\frac{T_c - T}{T_c}\right)^{\frac{1}{2\kappa}}, \tag{3.32}$$

$$\mathrm{Var}(m)_\kappa \simeq \pm\left(\frac{2\kappa\langle G^2\rangle}{\langle G^{2+2\kappa}\rangle}\right)^{\frac{1}{\kappa}}(\langle G^2\rangle - 1)\left(\frac{T_c - T}{T_c}\right)^{\frac{1}{\kappa}}, \tag{3.33}$$

valid whenever $\langle G^{2+2\kappa}\rangle$ is finite. Thus, the critical exponents are $\lambda_1 = 1/2\kappa$ and $\lambda_2 = 1/\kappa$. Remarkably, we see that the critical exponents of long-ranged mean-field Ising systems are sensitive to the tails of the distribution of threshold noise and that $\kappa = 1$ reproduces the critical behaviour of $\mu_h(\zeta)$. Equations (3.32) and (3.33) are compared with the numerical solution of the fixed point equations (3.15) and (3.16) in figure 3.1.4, showing excellent agreement.

3.2 Dynamical behaviour

Equations (2.42), (2.46) and (2.48) describe the macroscopic dynamics of the system given a set of initial conditions for the local magnetizations $m_{1,0}, \cdots, m_{N,0}$ and u_0. We

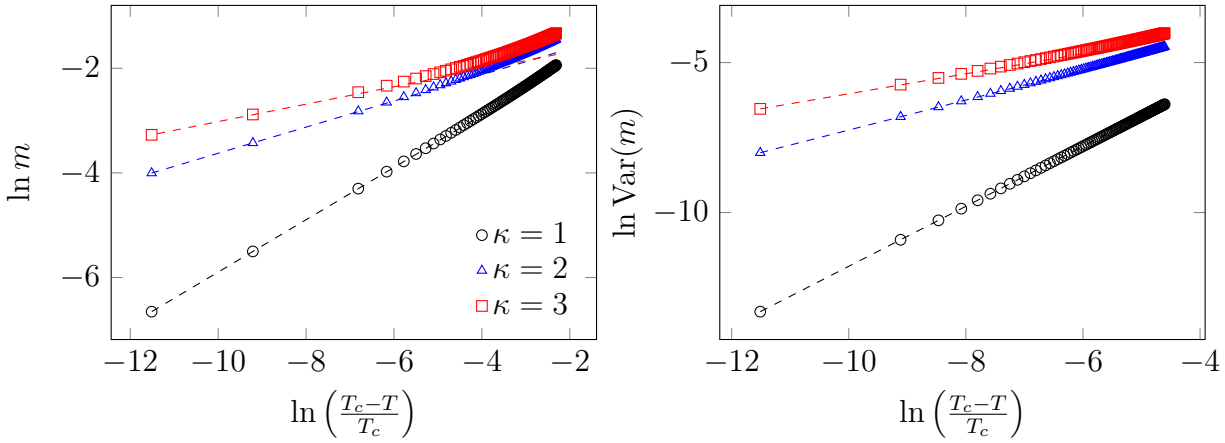

Figure 3.1.4 – Global magnetization m and variance of $\mathcal{P}(m)$ as a function of the reduced temperature $\frac{T-T_c}{T_c}$ for a random graphs with negative binomial degree distribution with variance $\Delta^2 = \frac{1}{\alpha}$. Symbols denote the solution of the fixed point equations (3.15) and (3.16), while dashed lines represent the analytic expressions (3.32) (left) and (3.33) (right), for the algebraic threshold noise distribution μ_κ, equation (3.6), with different values of κ and $\alpha = 1$.

consider homogeneous initial conditions $m_{i,0} = m_0$, for any i, implying that $u_0 = m_0$ from equation (2.44). Figure 3.2.1 illustrates the evolution of the global magnetization in the ferromagnetic phase for $T = T_c/2$. Dashed lines represent the iterative map of equations (2.42) and (2.46), while symbols are the results obtained from simulations of the microscopic dynamics given by equation (2.3). The theoretical results and the simulations are in excellent agreement. A comparison between dynamics for the configuration model and for the equivalent fully connected graph, generated through equation (2.55), is presented in the inset for a large network. As mentioned in Chapter 2, the equivalence between these two models leads to a practical advantage, since it is computationally cheaper to simulate a fully connected weighted network than the correspondent configuration model for large c, as well as it suggests a relation between the adjacency matrix eigenspectrum and the dynamical process happening on top of the network, being the former the context in which this equivalence was formally proven [56].

First, we characterize the dynamical behavior at the critical temperature, in terms of the dynamical critical exponent for the magnetization, introduced in Section 2.3. We also compute the analogous dynamical exponent for the variance of $\mathcal{P}(m)$. For long times $t \gg 1$, m_t and $\mathrm{Var}(m_t)$ behave as

$$m_t \propto t^{-z_1}, \tag{3.34}$$

$$\mathrm{Var}(m_t) \propto t^{-z_2}. \tag{3.35}$$

Figures 3.2.2 and 3.2.3 illustrate, respectively, the dynamics of m_t and $\mathrm{Var}(m_t)$ at $T = T_c$, for different initial conditions and different threshold noise distributions. After an initial transient behavior, which depends on the initial condition, the quantities display the

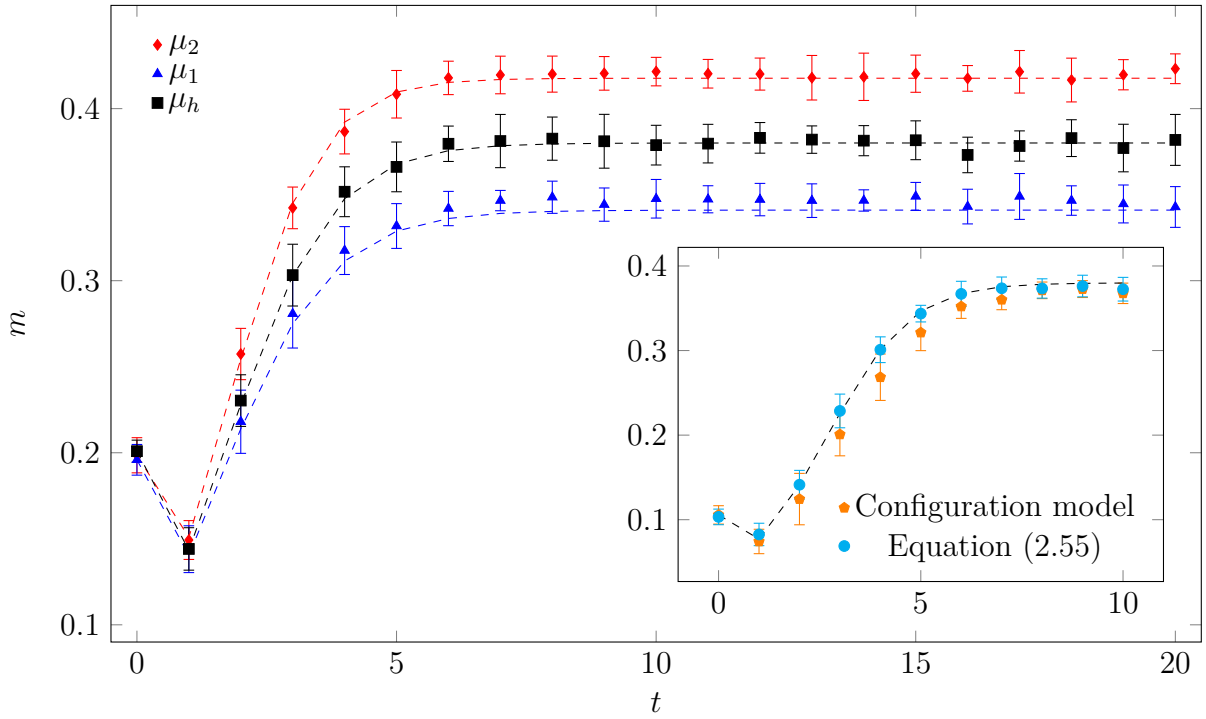

Figure 3.2.1 – Dynamics of the global magnetization in the ferromagnetic phase for $T = \frac{T_c}{2}$ and $\alpha = 0.625$. Dashed lines represent the solution of the iterative equations (2.42) and (2.46) for the negative binomial degree distribution, while symbols denote numerical simulations obtained from equation (2.3). The vertical bars are the standard deviation obtained from 10 simulations of a graph generated according to equation (2.55) with $N = 10^4$ and $c = 10^2$. The main panel shows a comparison between our theoretical equations and simulations for different threshold noise distributions, while the inset presents a comparison between the dynamics with the configuration model and the equivalent fully connected configuration (2.55) for the hyperbolic threshold noise μ_h, equation (3.5).

following asymptotic behavior

$$m_t^{(h)} \propto t^{-\frac{1}{2}}, \quad \mathrm{Var}(m_t) \propto t^{-1}, \tag{3.36}$$

$$m_t^{(\kappa)} \propto t^{-\frac{1}{2\kappa}}, \quad \mathrm{Var}(m_t)^{(\kappa)} \propto t^{-\frac{1}{\kappa}}. \tag{3.37}$$

The dynamical exponents for the hyperbolic threshold noise, namely $z_1 = 1/2$ and $z_2 = 1$, are in accordance with the mean field dynamical exponents for purely dissipative systems with no conserved order parameter [51, 57]. Interestingly, similar to the results for the stationary regime, the dynamical exponents, $z_1 = 1/2\kappa$ and $z_2 = 1/\kappa$, depend on the tails of the algebraic distribution of threshold noise, which is in contrast with the usual mean-field results. We also see that the dynamical critical exponents have the same values as their stationary counterparts, for both distributions of the threshold noise (see equations (3.29-3.33)). In figure 3.2.4 we confirm that the universal long time exponents

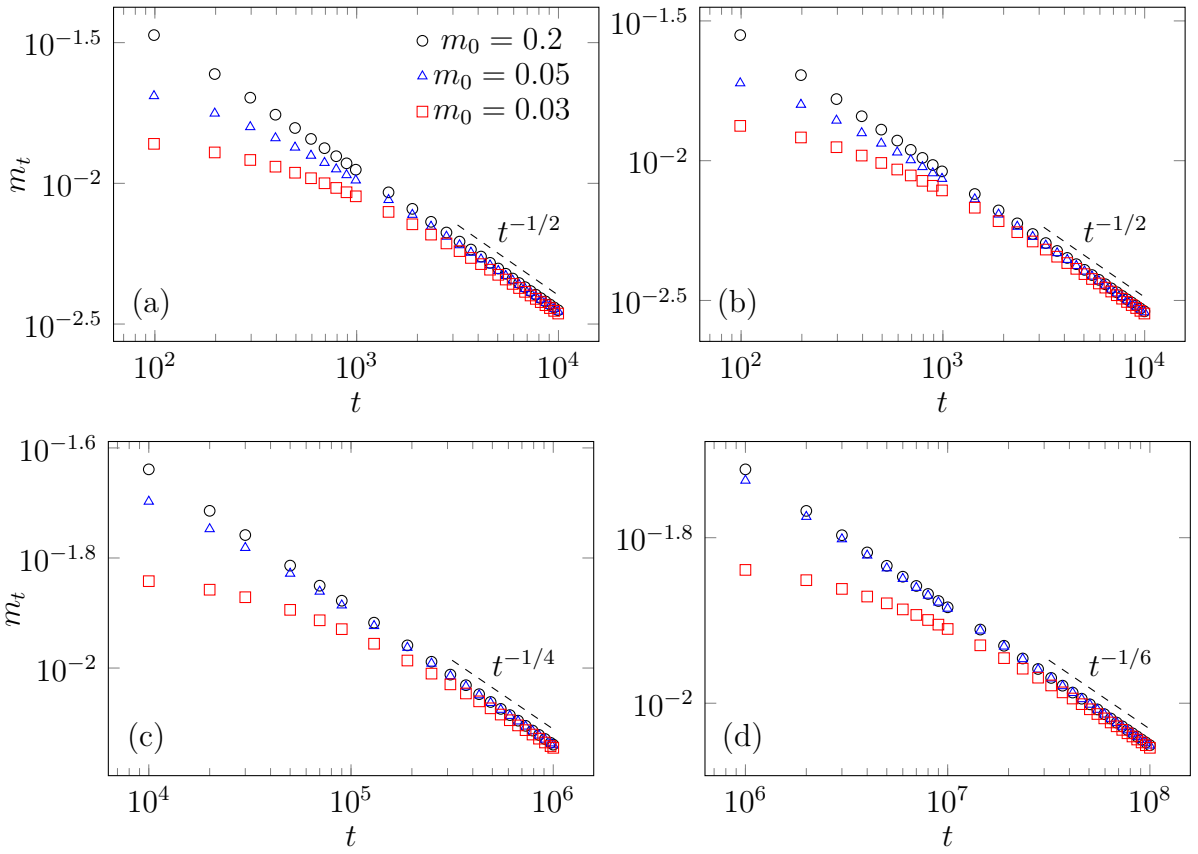

Figure 3.2.2 – Dynamics of the global magnetization m_t at the critical temperature $T = T_c$, obtained from equations (2.42) and (2.46), for $\alpha = 1$ and (a) hyperbolic, (b) $\kappa = 1$, (c) $\kappa = 2$ and (d) $\kappa = 3$ algebraic threshold noise distributions. Symbols denote the values for different initial magnetizations and the dashed lines are the slopes of the magnetization for long time behavior, $z_1 = 1/2$ for μ_h and $z_1 = 1/2\kappa$ for μ_κ.

are independent of degree distributions by presenting the long time behavior of m_t and $\mathrm{Var}(m_t)$ for different distributions of the threshold noise and different values of α.

Finally, we study the effect of degree fluctuations and of the threshold noise on the dynamics inside each phase. For a given initial condition $0 < m_0 < 1$, the system relaxes exponentially fast to the stationary magnetization m in the long time regime as

$$|m_t - m| \propto e^{-\frac{t}{\tau}}, \tag{3.38}$$

where τ is the relaxation time, a measure of how long it takes for the system to reach its stationary state. In general, τ is a function of α and T. Figure 3.2.5 shows $\tau(\alpha)$ for fixed $T/J = 2$ and $\tau(T)$ for fixed $\alpha = 1$. We see that $\tau(\alpha) \propto |\alpha - \alpha_c|^{-1}$ and $\tau(T) \propto |T - T_c|^{-1}$, approaching the critical point from any phase independently of the noise threshold, showing that $Z = 2$ for the dynamical critical exponent. Thus, the dynamical critical exponent that governs the divergence of the relaxation time is given by $Z = 2$, independently of the degree distribution and the threshold noise distribution. This result agrees with the satandard mean-field critical behaviors.

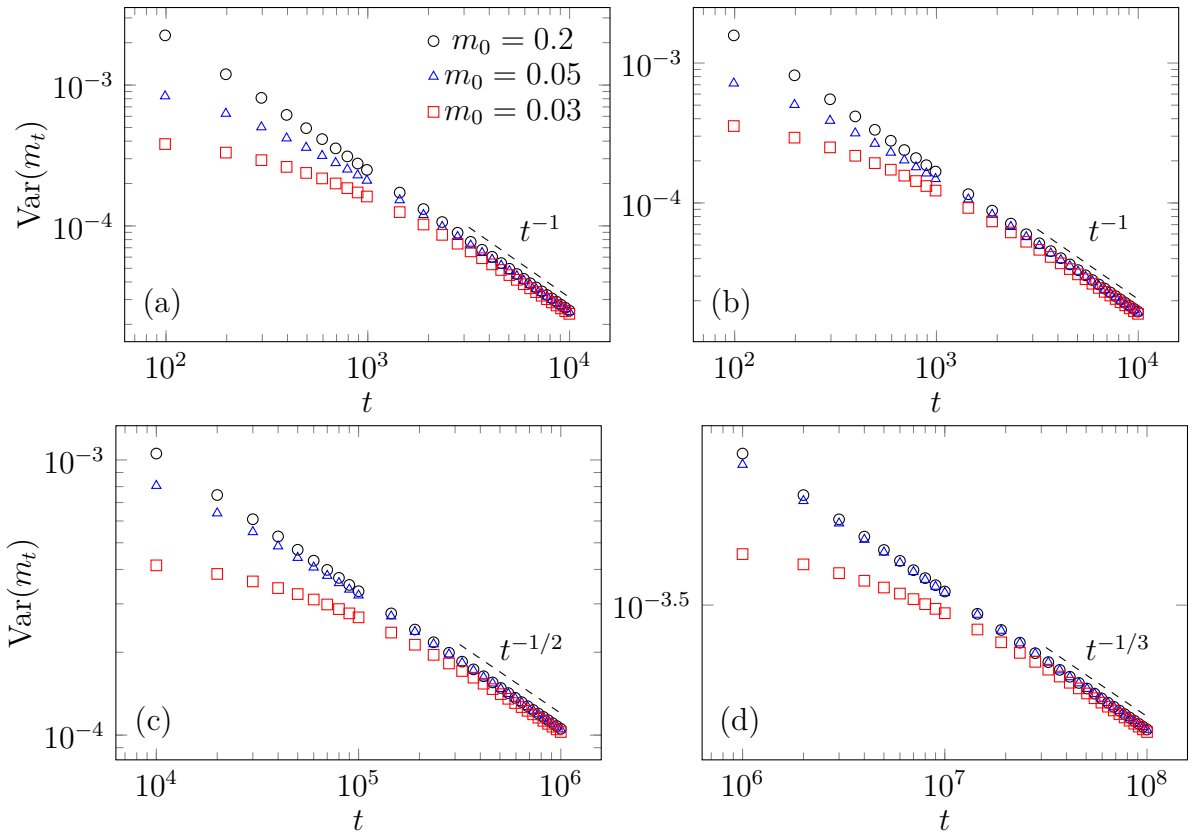

Figure 3.2.3 – Variance of local magnetizations $\mathrm{Var}(m_t)$ at the critical temperature $T = T_c$, obtained from equation (3.26), for $\alpha = 1$ and (a) hyperbolic, (b) $\kappa = 1$, (c) $\kappa = 2$ and (d) $\kappa = 3$ algebraic noise thresholds. Symbols denote the values for different initial magnetizations and the dashed line denote the slopes that characterize the long time behaviors, $z_2 = 1$ for μ_h, equation (3.5), and $z_2 = 1/\kappa$ for μ_κ, equation (3.6).

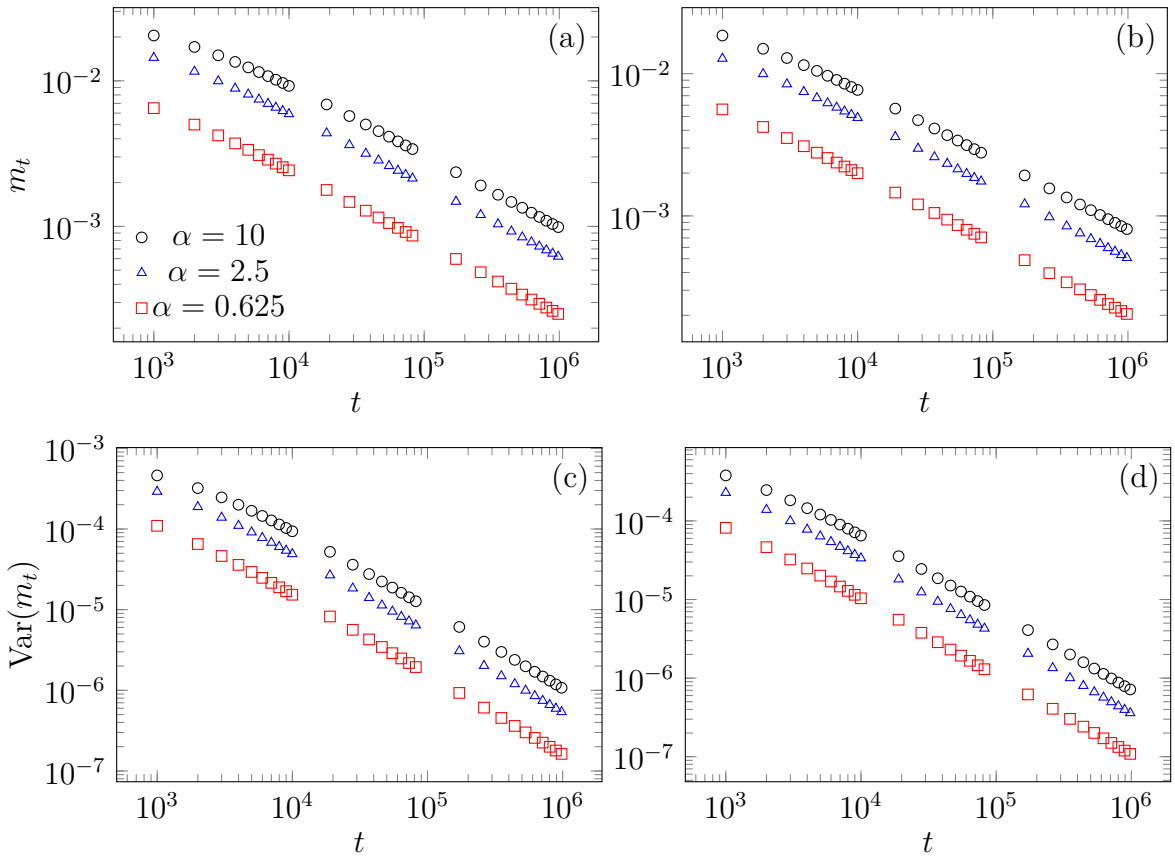

Figure 3.2.4 – Long time dynamics of the global magnetization m_t, obtained from equations (2.42) and (2.46) and of the variance of $\mathcal{P}_t(m)$, $\mathrm{Var}(m)$, from equation (3.26), for μ_h, (a) and (c), and μ_κ, (b) and (d), with $\kappa = 1$. All magnetization curves have slope equal to $1/2$, while $\mathrm{Var}(m)$ curves have slope equal to 1. The system is defined over a random graph with a negative binomial degree distribution, equation (2.43), with variance $\Delta_\nu = \frac{1}{\alpha}$.

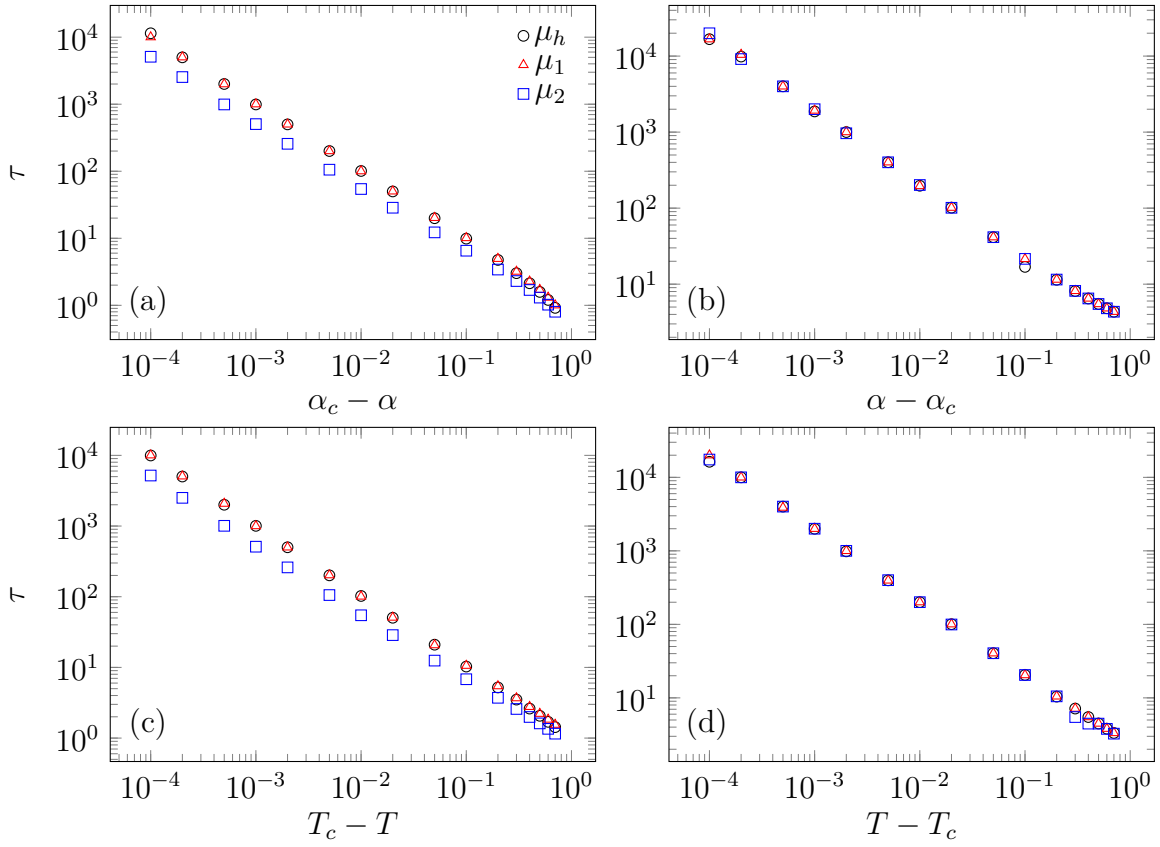

Figure 3.2.5 – Relaxation time τ as a function of α for fixed $T = 2J$ and $\alpha_c = 1$, (a) and (b), and as a function T for fixed $\alpha = 1$ with $T_c = 2J$, (c) and (d), according to equation (3.19) for different noise thresholds. All curves have slope equal to 1. The system is defined over a random graph with a negative binomial degree distribution, equation (2.43), with variance $\Delta_\nu = \frac{1}{\alpha}$.

4 Conclusion

In conclusion, we presented an exact solution for the dynamics of the Ising model on heterogeneous and highly connected complex networks, with an arbitrary threshold noise distribution. Based on the Markov process associated to the spin update rule known as parallel Glauber dynamics, equation (2.3), we make use of the law of large numbers to obtain a set of dynamical equations for the global magnetization of the system, equations (2.42) and (2.46), alternatively derived through the consolidated generating functional approach in Appendix A. In addition, we derived the full distribution of local magnetizations for each time step of the discrete dynamics, equation (2.48). The generality of the formalism allows to characterize both dynamical and stationary phenomena in terms of any degree distribution with non-diverging moments and to explore the role of the heat bath in the dynamics, emulated by the threshold noise distribution.

Both dynamical and stationary results are validated by numerical simulations, based on the stochastic single spin update rule. The results for the dynamics presented in the inset of figure 3.2.1 show the equivalence, in the high connectivity limit, between the interaction matrix of the Ising model on configuration graphs and the fully connected weighted ensemble, given by relation (2.55). This equation allows to simulate large networks without the necessity of more sophisticated algorithms to generate random graphs.

We presented results for the negative binomial degree distribution, equation (3.1), whose high connectivity limit is characterized solely by the variance of the rescaled degree distribution $\Delta^2 = \frac{1}{\alpha}$. By making this choice, we are able to easily interpolate between heterogeneous and homogeneous regimes through variation of the parameter $\alpha > 0$. We have shown that the system undergoes a continuous phase transition between ferromagnetic and paramagnetic phases, and that the critical temperature is independent of the tail of the threshold noise distribution, being affected only by its behavior near zero. As the variance of the rescaled degree distribution vanishes ($\alpha \to \infty$), we recover the well known behavior of fully connected systems, which defines a universality class for homogeneous networks. In the strongly heterogeneous limit, as $\Delta^2 \to \infty$ (or $\alpha \to 0$), the critical temperature diverges, therefore the system lies in a ferromagnetic phase for any finite value of temperature.

The reasons for the specific choices of threshold noise distribution, equations (3.5) and (3.6), were two. The first is related to the slow tail of the algebraic distribution. Through comparison with the fast exponential decaying of the hyperbolic threshold noise, we investigated the effects of strong thermal fluctuations, promoted by the slower power law tail of the algebraic noise threshold. The second reason concerns the stationary microstate distribution and detailed balance. When the stationary form of the microstate probability is not Boltzmann-like, which is the case for most choices of threshold noise distribution,

detailed balance does not hold. By deriving the explicit form of the stationary microstate probability in the high connectivity limit, equation (3.10), we show that it is Boltzmann-like for the hyperbolic tangent case, while it is not for the algebraic one. The fact that our theory allows to study systems for which detailed balance does not hold is an important result, since one can use the fixed point limit of the dynamical equations to study stationary states that are not accessible to equilibrium statistical mechanics.

We focused on the characterization of critical phenomena, both stationary and dynamical, in terms of critical exponents. We obtained the stationary critical exponents for the global magnetization and for the variance of the local magnetizations, as $T \to T_c$. For the hyperbolic threshold noise, detailed balance holds and we recover the usual mean-field critical exponents, while for the algebraic threshold the critical exponents are explicit functions of the natural parameter κ, that controls the tail of the noise distribution. Since fluctuations in the local magnetizations are not present in homogeneous ferromagnetic Ising models, we compare the critical exponents for $\mathrm{Var}(m)$ with the fully connected spin glass, or Sherrington-Kirkpatrick model. Our results show that the variance of $\mathcal{P}(m)$ vanishes linearly with the rescaled temperature $\frac{T_c - T}{T}$ for the hyperbolic activation, exactly as the variance of the distribution of local fields for the replica symmetric solution of the aforementioned model. As happened to the global magnetization, the algebraic threshold noise distribution induce tail dependence on the critical exponents of $\mathrm{Var}(m)$.

Regarding dynamical critical phenomena, we obtained the long time exponents for the relaxation of the global magnetization, m_t, and for $\mathrm{Var}(m_t)$. Again, the hyperbolic threshold noise distribution promotes the same exponents as usual homogeneous mean-field theories, while the algebraic distribution introduces tail dependence. Finally, we characterized the divergence of the relaxation time as $|T \to T_c|$ and as $|\alpha \to \alpha_c|$. In both cases, the power law divergence is linear, in accordance with previous results that relate τ to the stationary correlation length ξ.

As open problems and future perspectives, our work raises some interesting questions. Since our derivation is based on the law of large numbers, degree distributions with divergent moments, such as scale free networks, are not contemplated *a priori*, so it would be interesting to investigate such cases. Another natural generalization of our theory would be the sequential version of the dynamics, that allows to investigate short time behavior and its closer to physical phenomena.

Overall, our work introduces a family of Ising models on random graphs that retain the effect of both topological structure and noise distribution, and whose non-equilibrium dynamics can be solved exactly, presenting insights on the network effect on the dynamics representing a step further in the direction of the understanding of real complex network phenomena, where finite connectivity and degree fluctuations are of vital importance. Through characterization of critical exponents, our results show that the details of the microscopic evolution are relevant factors in determining critical phenomena in non equi-

librium systems and that detailed balance recovers usual mean field behavior.

Appendices

A Generating functional formalism

In this appendix we present the derivation of the dynamical map given by equations (2.42) and (2.46) through the consolidated generating functional method [40] or Martin-Siggia-Rose path integral formalism [48]. The standart approach of this derivation is to consider the configuration model [42, 58], but the equivalence relation between this model and the fully connected adjacency matrix given by (2.55) in Chapter 2 allow to a more straightforward derivation, so we will adopt it here.

Considering the evolution of the state vector $\boldsymbol{\sigma}$ through phase space, from an initial time set to 0 to a final time t, the generating functional $Z[\boldsymbol{\psi}]$ is given by

$$Z[\boldsymbol{\psi}] = \left\langle e^{-i\sum_{s=0}^{t}\boldsymbol{\psi}_s\cdot\boldsymbol{\sigma}_s} \right\rangle, \tag{A.1}$$

where $\langle\cdots\rangle$ denote phase space average and $\boldsymbol{\psi}$ is an auxiliary field that yield the all moments of the spin variables, in particular the magnetization

$$m_t = \lim_{N\to\infty}\frac{i}{N}\sum_{j=1}^{N}\frac{\partial}{\partial\psi_{j,s}}Z[\boldsymbol{\psi}]\Big|_{\{\boldsymbol{\psi}_s\}=0}, \tag{A.2}$$

where $\{\boldsymbol{\psi}_s\} = 0$ denotes $\psi_{j,t} = 0$ for any j and t. For a discrete path of the spin system, this average is written in terms of the transition matrix elements (2.14) as

$$Z[\boldsymbol{\psi}] = \sum_{\boldsymbol{\sigma}_0\cdots\boldsymbol{\sigma}_t} p(\boldsymbol{\sigma}_0)\prod_{j=1}^{N} e^{-i\sum_{s=0}^{t}\psi_{j,s}\sigma_{j,s}}\prod_{s=0}^{t-1}\frac{1}{2}\{1+\sigma_{j,s+1}\mathcal{F}[\beta h_j(\boldsymbol{\sigma}_s)]\}. \tag{A.3}$$

To introduce the analytical forms of the local fields (2.5) with an extra term $G_j\theta_{j,s}$, we use the Dirac-δ integral identities

$$1 = \int\left(\prod_{j=1}^{N}\prod_{s=0}^{t-1}\frac{dh_{j,s}d\hat{h}_{j,s}}{2\pi}e^{i\hat{h}_{j,s}\left[h_{j,s}-\frac{J}{c}\sum_{l\in\partial_j}\sigma_{l,s}-G_j\theta_{j,s}\right]}\right), \tag{A.4}$$

where the single integral symbol denotes integration over h and $\hat{h}$ from $-\infty$ to $+\infty$. This additional term in the local fields will be used later to get rid of spurious order parameters. Since

$$\frac{J}{c}\sum_{l\in\partial_j}\sigma_{l,s} = \frac{J}{c}\sum_{l=1}^{N}C_{jl}\sigma_{l,s} = \frac{J}{N}G_j\sum_{l=1}^{N}G_l\sigma_{l,s}, \tag{A.5}$$

where we made use of the high-connectivity equivalence (2.55), topological disorder is explicitly introduced in the generating functional through local fields, resulting in

$$Z[\boldsymbol{\psi}] = \sum_{\boldsymbol{\sigma}_0\cdots\boldsymbol{\sigma}_t} p(\boldsymbol{\sigma}_0)e^{-i\sum_{j=1}^{N}\sum_{s=0}^{t}\psi_{j,s}\sigma_{j,s}}\times$$
$$\times\int\left(\prod_{j=1}^{N}\prod_{s=0}^{t-1}\frac{dh_{j,s}d\hat{h}_{j,s}}{4\pi}e^{ih_{j,s}\hat{h}_{j,s}}\left\langle e^{-\frac{i}{N}\hat{h}_{j,s}JG_j\sum_{l=1}^{N}G_l\sigma_{l,s}-iG_j\hat{h}_{j,s}\theta_{j,s}}\left[1+\sigma_{j,s+1}\mathcal{F}(\beta h_{j,s})\right]\right\rangle_{\boldsymbol{G}}\right), \tag{A.6}$$

where the average over $\boldsymbol{G} = (G_1, \ldots, G_N)$ is taken in order to count for all possible realizations of the network. In the previous expression, sites are coupled through the rescaled degrees, so in order to proceed with the evaluation of the average, we decouple them by introducing the parameters

$$u_s = \frac{1}{N}\sum_{j=1} G_j \sigma_{j,s}, \tag{A.7}$$

$$v_s = \frac{1}{N}\sum_{j=1} G_j \hat{h}_{j,s}, \tag{A.8}$$

via integral identities similar to (A.4), yielding the compact form

$$Z[\boldsymbol{\psi}] = \int \left(\prod_{s=0}^{t-1} \frac{N^2 du_s d\hat{u}_s dv d\hat{v}_s}{4\pi^2} \right) e^{N\Phi(u,\hat{u},v,\hat{v})}, \tag{A.9}$$

with

$$\Phi(u,\hat{u},v,\hat{v}) = i\sum_{s=0}^{t-1}[\hat{u}_s u_s + \hat{v}_s v_s - J u_s v_s] + \\ + \frac{1}{N}\sum_{j=1}^{N} \ln\left\{ \sum_{\vec{\sigma}} e^{-i\sum_{s=0}^{t}\psi_{j,s}\sigma_s} \int \prod_{s=0}^{t-1} \frac{dh_s d\hat{h}_s}{2\pi} \left\langle \mathcal{M}(h_s,\hat{h}_s,\sigma_s) \right\rangle_G \right\}, \tag{A.10}$$

where

$$\mathcal{M}(h_s,\hat{h}_s,\sigma_s) = e^{i\hat{h}_s[h_s - G\theta_{j,s}] - iG(\hat{u}_s\sigma_s + \hat{v}_s\hat{h}_s)} \frac{1}{2}\left[1 + \sigma_{s+1}\mathcal{F}(\beta h_s)\right]. \tag{A.11}$$

The index omission in last equation is due to the fact that for every site, we carry summations over all possible values of σ and integrate over all possible values of $\hat{h}, h$ and G, therefore the generating functional is site dependent only through the auxiliary fields $\boldsymbol{\psi}_s$ and $\boldsymbol{\theta}_s$. In the thermodynamic limit, equation (A.9) can be evaluated by the saddle point method as

$$\lim_{N\to\infty} Z[\boldsymbol{\psi}] = e^{N\Phi_*}, \tag{A.12}$$

being Φ_* the functional (A.10) evaluated at the saddle point of the manifold spammed by the order parameters, where by definition, differentiation with respect to coordinates is zero. Making use of this fact, together with the normalization condition $Z[\boldsymbol{\psi} = 0] = 1$, differentiation of (A.12) with respect to order parameters yields

$$\hat{u}_t = J v_t, \tag{A.13}$$

$$\hat{v}_t = J u_t. \tag{A.14}$$

Similarly, differentiation with respect to conjugate order parameters in the limit of $\boldsymbol{\psi}, \boldsymbol{\theta} \to 0$ yields

$$u_t = \frac{\sum_{\vec{\sigma}} \int \prod_{s=0}^{t-1} \frac{dh_s d\hat{h}_s}{2\pi} \left\langle \mathcal{M}(h_s,\hat{h}_s,\sigma_s) G\sigma_t \right\rangle_G}{\sum_{\vec{\sigma}} \int \prod_{s=0}^{t-1} \frac{dh_s d\hat{h}_s}{2\pi} \left\langle \mathcal{M}(h_s,\hat{h}_s,\sigma_s) \right\rangle_G}, \tag{A.15}$$

$$v_t = \frac{\sum_{\vec{\sigma}} \int \prod_{s=0}^{t-1} \frac{dh_s d\hat{h}_s}{2\pi} \left\langle \mathcal{M}(h_s,\hat{h}_s,\sigma_s) G\hat{h}_t \right\rangle_G}{\sum_{\vec{\sigma}} \int \prod_{s=0}^{t-1} \frac{dh_s d\hat{h}_s}{2\pi} \left\langle \mathcal{M}(h_s,\hat{h}_s,\sigma_s) \right\rangle_G}, \tag{A.16}$$

and from equation (A.2), the magnetization is obtained as

$$m_t = \frac{\sum_{\vec{\sigma}} \int \prod_{s=0}^{t-1} \frac{dh_s d\hat{h}_s}{2\pi} \Big\langle \mathcal{M}(h_s, \hat{h}_s, \sigma_s)\sigma_t \Big\rangle_G}{\sum_{\vec{\sigma}} \int \prod_{s=0}^{t-1} \frac{dh_s d\hat{h}_s}{2\pi} \Big\langle \mathcal{M}(h_s, \hat{h}_s, \sigma_s) \Big\rangle_G}. \tag{A.17}$$

To obtain the explicit forms of u_t and m_t, we must be able to carry out the averages involving $\mathcal{M}(h_s, \hat{h}_s, \sigma_s)$. Until now, all we did was conveniently multiply the original definition of the generating functional by one, therefore equations (A.9) and (A.1) are equals, and since the latter is not a function of $\boldsymbol{\theta}$, the following identity holds

$$\frac{\partial}{\partial \theta_{j,t}} Z[\boldsymbol{\psi}] = \frac{\sum_{\vec{\sigma}} \int \prod_{s=0}^{t-1} \frac{dh_s d\hat{h}_s}{2\pi} \Big\langle \mathcal{M}(h_s, \hat{h}_s, \sigma_s) G\hat{h}_t \Big\rangle_G}{\sum_{\vec{\sigma}} \int \prod_{s=0}^{t-1} \frac{dh_s d\hat{h}_s}{2\pi} \Big\langle \mathcal{M}(h_s, \hat{h}_s, \sigma_s) \Big\rangle_G} = 0, \tag{A.18}$$

rendering $v_t = 0$ for any t. This result in yields the normalization

$$\sum_{\vec{\sigma}} \int \prod_{s=0}^{t-1} \frac{dh_s d\hat{h}_s}{2\pi} \Big\langle \mathcal{M}(h_s, \hat{h}_s, \sigma_s) \Big\rangle_G = 1, \tag{A.19}$$

that allow the determination of u_t and m_t as

$$u_t = \Big\langle G\mathcal{F}(\beta J G u_{t-1}) \Big\rangle_G, \tag{A.20}$$

$$m_t = \Big\langle \mathcal{F}(\beta J G u_{t-1}) \Big\rangle_G. \tag{A.21}$$

Since the variables G are sorted from $\nu(g)$, changing $t \to t+1$ yields the dynamical map given by (2.46) and (2.42).

B Change of variables

In this appendix, we discuss in more detail the method to obtain the distribution of a function of a random variable, known as change of variables.

Let X be a random variable drawn from a known distribution $f_X(x)$, and $Y = \mathcal{F}(X)$ a function of X. Immediatly, we can establish the following identity

$$p(X = x) = p(\mathcal{F}(X)) = \mathcal{F}(x)) = p(Y = y). \tag{B.1}$$

Since $P(X = x) = f_X(x)dx$, follows from the identity that

$$f_X(x)dx = f_Y(y)dy, \tag{B.2}$$

and therefore

$$f_Y(y) = \left|\frac{dx}{dy}\right| f_X(x), \tag{B.3}$$

where the absolute value is taken in order to count for substitutions of the form $Y = \mathcal{F}(X) = -X$. Now, since $x = \mathcal{F}^{-1}(y)$ by definition, where $\mathcal{F}^{-1}$ is the inverse of $\mathcal{F}$, we may write the last equation as

$$f_Y(y) = \left|\frac{d}{dy}\mathcal{F}^{-1}(y)\right| f_X[\mathcal{F}^{-1}(y)]. \tag{B.4}$$

Finally, from the property of inverse functions

$$\mathcal{F}^{-1}(ax) = \frac{1}{a}\mathcal{F}^{-1}(x), \tag{B.5}$$

we have

$$f_Y(y) = \frac{1}{a}\left|\frac{d}{dy}\mathcal{F}^{-1}(y)\right| f_X\left[\frac{\mathcal{F}^{-1}(y)}{a}\right]. \tag{B.6}$$

Now, recalling equation (2.47), namely

$$m_{i,t+1} = \mathcal{F}(J\beta G_i u_t), \tag{B.7}$$

we see that the local magnetization of spin i at time $t + 1$ is a function of the random variable G_i, drawn from the known distribution $\nu(g)$. From equation (B.6), identifying $a = \beta J u_t$, $x = g$ and $y = m$, equation (2.48) for the distribution of local magnetizations $\mathcal{P}_t(m)$ is recovered.

C Rescaled degree distributions

In this appendix, we present the derivation of the rescaled distributions of the Erdős-Rényi ensemble and for the configuration model with negative binomial degree distribution.

The Erdős-Rényi model consists of random graphs denoted by $G(N,p)$, where N is the number of edges and p is the probability that an arbitrary pair of nodes is connected. For finite N, the degree distribution $p_k^{(\mathrm{ER})}$ of a random graph of this ensemble is the binomial distribution [14]

$$p_k^{(\mathrm{ER})} = \binom{N-1}{k} p^k (1-p)^{N-1-k}, \tag{C.1}$$

where $\binom{y}{x}$ is the binomial coefficient. Fixing $c = Np$ as constant, in the thermodynamic limit, the binomial distribution converges to the Poisson's distribution, yielding

$$p_k^{(\mathrm{ER})} = \frac{c^k e^{-c}}{k!}. \tag{C.2}$$

Now, from the definition of the rescaled distribution, equation (2.43), we have

$$\nu(g)^{(\mathrm{ER})} = \lim_{c\to\infty} \sum_{k\geq 0} \frac{c^k e^{-c}}{k!} \delta\left(g - \frac{k}{c}\right). \tag{C.3}$$

Through the integral form of Dirac's delta,

$$\delta(x-y) = \frac{1}{2\pi} \int_{-\infty}^{\infty} d\omega e^{-i\omega(x-y)}, \tag{C.4}$$

we may write

$$\nu(g)^{(\mathrm{ER})} = \lim_{c\to\infty} \frac{1}{2\pi} \int_{-\infty}^{\infty} d\omega e^{i\omega g} e^{-c} \sum_{k\geq 0} \frac{c^k}{k!} e^{-i\frac{\omega k}{c}}. \tag{C.5}$$

This summation can be directly solved, noting that

$$\sum_{k\geq 0} \frac{c^k}{k!} e^{-i\frac{\omega k}{c}} = \sum_{k\geq 0} \frac{1}{k!} \left(ce^{\frac{-i\omega}{c}}\right)^k = e^{ce^{-i\frac{\omega}{c}}}, \tag{C.6}$$

resulting in

$$\nu(g)^{(\mathrm{ER})} = \lim_{c\to\infty} \frac{1}{2\pi} \int_{-\infty}^{\infty} d\omega e^{i\omega g} e^{-c} e^{ce^{-i\frac{\omega}{c}}}. \tag{C.7}$$

By considering c large we may approximate

$$e^{-i\frac{\omega}{c}} \approx 1 - \frac{i\omega}{c}, \tag{C.8}$$

obtaining the final form

$$\nu(g)^{(\mathrm{ER})} = \frac{1}{2\pi} \int_{-\infty}^{\infty} d\omega e^{-i\omega(g-1)} = \delta(g-1), \tag{C.9}$$

so we see that, in the high connectivity limit, by first taking $N \to \infty$ and then $c \to \infty$, the Erdős-Rényi ensemble is homogeneous, once its rescaled degree distribution is a Delta distribution, with null variance $\Delta^2_{\mathrm{ER}} = 0$.

Now for the negative binomial configuration graph, the form of the degree distribution at the thermodynamic limit is equation (2.26), namely

$$p_k^{(\mathrm{NB})} = \frac{\Gamma(\alpha+k)}{k!\Gamma(\alpha)} \left(\frac{c}{\alpha}\right)^k \left(\frac{\alpha}{\alpha+c}\right)^{\alpha+k}. \tag{C.10}$$

Its rescaled degree distribution can be written as

$$\nu(g)^{(\mathrm{NB})} = \frac{\alpha^\alpha}{\Gamma(\alpha)} \lim_{c\to\infty} \sum_{k\geq 0} \frac{c^k}{(\alpha+c)^{\alpha+k}} \frac{\Gamma(\alpha+k)}{k!} \delta\left(g - \frac{k}{c}\right), \tag{C.11}$$

and again making use of the Dirac's delta identity (C.4), we have

$$\nu(g)^{(\mathrm{NB})} = \frac{\alpha^\alpha}{\Gamma(\alpha)} \frac{1}{2\pi} \int_{-\infty}^{\infty} d\omega e^{i\omega g} \lim_{c\to\infty} (\alpha+c)^{-\alpha} \sum_{k\geq 0} \left[\frac{ce^{-i\frac{\omega}{c}}}{(\alpha+c)}\right]^k \frac{\Gamma(\alpha+k)}{k!}. \tag{C.12}$$

Using the integral definition of the gamma function,

$$\Gamma(x) = \int_0^\infty d\gamma\, \gamma^{x-1} e^{-\gamma}, \tag{C.13}$$

the summation on the previous equation may be written as

$$\int_0^\infty d\gamma \gamma^{\alpha-1} e^{-\gamma} \sum_{k\geq 0} \frac{1}{k!} \left[\frac{\gamma c e^{-i\frac{\omega}{c}}}{(\alpha+c)}\right]^k = \int_0^\infty d\gamma \gamma^{\alpha-1} e^{-\gamma} e^{\frac{\gamma c e^{-i\frac{\omega}{c}}}{(\alpha+c)}}, \tag{C.14}$$

whose solution, *vide* integral 3.351.1 Gradstheyn and Rhyzik's table of Integrals, Series and Products [55] is

$$\int_0^\infty d\gamma \gamma^{\alpha-1} e^{-\gamma} e^{\frac{\gamma c e^{-i\frac{\omega}{c}}}{(\alpha+c)}} = \Gamma(\alpha) \left(\frac{\alpha+c}{\alpha+c-ce^{-i\frac{\omega}{c}}}\right)^\alpha. \tag{C.15}$$

Combining the last result with equation (C.12), we have for the rescaled degree distribution

$$\nu(g)^{(\mathrm{NB})} = \frac{\alpha^\alpha}{2\pi} \int_{-\infty}^{\infty} d\omega (\alpha + c - ce^{-i\frac{\omega}{c}})^{-\alpha} e^{i\omega g}, \tag{C.16}$$

and by making use of the same approximation for large c, equation (C.8), we have

$$\nu(g)^{(\mathrm{NB})} = \frac{\alpha^\alpha}{2\pi} \lim_{c\to\infty} \int_{-\infty}^{\infty} d\omega \frac{e^{i\omega g}}{(\alpha+i\omega)^\alpha} = \frac{\alpha^\alpha}{\Gamma(\alpha)} g^{\alpha-1} e^{-\alpha g}, \tag{C.17}$$

vide integral 3.382.7 of Gradstheyn and Rhyzik's table of Integrals, Series and Products [55], recovering (3.3). Being $\langle G \rangle = 1$, as shown in equation (3.18), the variance of the rescaled distribution is given by

$$\Delta^2_{\mathrm{NB}} = \frac{\alpha^\alpha}{\Gamma(\alpha)} \int_0^\infty dg g^{\alpha+2} e^{-\alpha g} - 1. \tag{C.18}$$

Integrating by parts, we have

$$\Delta^2_{\mathrm{NB}} = \frac{\alpha^\alpha}{\Gamma(\alpha)} \left[-\frac{g^{\alpha+1} e^{-\alpha g}}{\alpha} \Bigg|_0^\infty + \frac{\alpha+1}{\alpha} \langle G \rangle \right] - 1 = \frac{1}{\alpha}, \tag{C.19}$$

recovering the result in equation (3.4). Therefore, we see that the negative binomial ensemble of configuration graphs is heterogeneous for finite α, and homogeneous in the limit of α going to infinity.

D Heterogeneous stationary critical exponents

In this appendix, we present the derivation of the stationary critical exponents for the hyperbolic activation, equations (3.29) and (3.30), and for the algebraic activation, equations (3.32) and (3.33).

For the hyperbolic activation $\mathcal{F}_h$, equation (3.7), we consider the second higher order on its Taylor expansion, namely

$$\tanh(x) \simeq x - \frac{x^3}{3}, \tag{D.1}$$

to write equation (2.46) as

$$u \simeq \int_0^\infty dg\, g\nu(g) \left[\beta J g u - \frac{1}{3}(\beta J g u)^3\right]. \tag{D.2}$$

In terms of the moments of the distribution $\nu(g)$, we may simplify this equation to

$$1 \simeq \beta J \langle G^2\rangle \left[1 - \frac{\langle G^4\rangle}{3\langle G^2\rangle}(\beta J u)^2\right]. \tag{D.3}$$

Now, through the identity

$$T = \left(1 + \frac{T - T_c}{T}\right) T_c, \tag{D.4}$$

we make use of the explicit form of the critical temperature, equation (3.19), to write

$$u = \frac{1}{\beta J}\left(\frac{3\langle G^2\rangle}{\langle G^4\rangle}\right)^{\frac{1}{2}} \left(\frac{T_c - T}{T_c}\right)^{\frac{1}{2}}. \tag{D.5}$$

As $u \to 0$, $\beta J \to (1 + \Delta_\nu^2)^{-1} = \langle G^2\rangle^{-1}$, yielding

$$u \simeq \left(\frac{3\langle G^2\rangle^3}{\langle G^4\rangle}\right)^{\frac{1}{2}} \left(\frac{T_c - T}{T_c}\right)^{\frac{1}{2}}. \tag{D.6}$$

Performing the same expansion up to the second higher order of the hyperbolic tangent in the fixed point expression for the magnetization, equation (2.42), we have

$$m \simeq \beta J u - \frac{\langle G^3\rangle}{3}(\beta J u)^3, \tag{D.7}$$

where we made use of the fact that $\langle G\rangle = 1$, as shown in equation (3.18). For very small u, the last equation is dominated by the term of $\mathcal{O}(u)$, that through subistitution of (D.6) results in

$$m \simeq \left(\frac{3\langle G^2\rangle}{\langle G^4\rangle}\right)^{\frac{1}{2}} \left(\frac{T_c - T}{T_c}\right)^{\frac{1}{2}}, \tag{D.8}$$

yielding the critical exponent presented in equation (3.29).

To determine the critical exponent for the variance $\mathrm{Var}(m)$, given by equation (3.26), we proceed similarly. Again, through the second higher order of the Taylor expansion of the hyperbolic tangent, we have

$$\mathrm{Var}(m) \simeq (\beta J u)^2(\langle G^2\rangle - 1) - \frac{2}{3}(\beta J u)^4\langle G^4\rangle + \frac{1}{9}(\beta J u)^6\langle G^6\rangle. \tag{D.9}$$

As $u \to 0$ and $(\beta J \to 1 + \Delta_\nu^2)^{-1} = \langle G^2\rangle^{-1}$, we consider the smaller order in u only and make use of equation (D.6) to finally obtain

$$\mathrm{Var}(m) \simeq \left(\frac{3\langle G^2\rangle}{\langle G^4\rangle}\right)(\langle G^2\rangle - 1)\left(\frac{T_c - T}{T_c}\right), \tag{D.10}$$

as given in equation (3.33).

For the algebraic activation $\mathcal{F}_\kappa$, we must perform the Taylor expansion in the variable $u^{2\kappa}$ in equation (2.46), in order to avoid the divergences of the expansion in the variable u. By doing so, the second higher order of the expansion yields

$$u \simeq \beta J u \int_0^\infty dg\, g^2 \nu(g)\left[1 - \frac{1}{2\kappa}(\beta J g u)^{2\kappa}\right]. \tag{D.11}$$

In terms of the moments of $\nu(g)$, we have

$$1 \simeq \beta J\langle G^2\rangle\left[1 - \frac{\langle G^{2+2\kappa}\rangle}{\langle G^2\rangle}\frac{(\beta J u)^{2\kappa}}{2\kappa}\right]. \tag{D.12}$$

From the identity in equation (D.4), we have

$$u \simeq \frac{1}{\beta J}\left(\frac{2\kappa\langle G^2\rangle}{\langle G^{2\kappa+2}\rangle}\right)^{\frac{1}{2\kappa}}\left(\frac{T_c - T}{T_c}\right)^{\frac{1}{2\kappa}}, \tag{D.13}$$

and again, as $u \to 0$ and $\beta J \to (1 + \Delta_\nu^2)^{-1} = \langle G^2\rangle^{-1}$, we obtain

$$u \simeq \left(\frac{2\kappa\langle G^2\rangle^{2\kappa+1}}{\langle G^{2\kappa+2}\rangle}\right)^{\frac{1}{2\kappa}}\left(\frac{T_c - T}{T_c}\right)^{\frac{1}{2\kappa}}. \tag{D.14}$$

Perfotming the same expansion in the variable $u^{2\kappa}$ on the fixed point equation for m, equation (3.15) for $\mathcal{F}_\kappa$, we obtain

$$m \simeq \beta J u - \frac{1}{2\kappa}(\beta J u)^{2\kappa}\langle G^{2\kappa}\rangle. \tag{D.15}$$

The smaller order of the last equation determines the critical exponent for the magnetization, through substitution of equation (D.14), as

$$m \simeq \left(\frac{2\kappa\langle G^2\rangle}{\langle G^{2+2\kappa}\rangle}\right)^{\frac{1}{2\kappa}}\left(\frac{T_c - T}{T_c}\right)^{\frac{1}{2\kappa}}, \tag{D.16}$$

as presented in equation (3.32).

For the critical exponent of $\mathrm{Var}(m)$, we have from equation (3.26)

$$\mathrm{Var}(m) \simeq (\beta J u)^2(\langle G^2\rangle - 1) - \frac{1}{\kappa}(\beta J u)^{2\kappa+2}\langle G^{2\kappa+2}\rangle + \frac{1}{4\kappa^2}(\beta J u)^{4\kappa+2}\langle G^{4\kappa+2}\rangle, \qquad \text{(D.17)}$$

where once more we considered the second order of the Taylor expansion in the variable $u^{2\kappa}$. Making use equation (D.14) as $u \to 0$ and $\beta J \to (1+\Delta_\nu^2)^{-1} = \langle G^2\rangle^{-1}$, the smaller order of the last equation yields the critical exponent for $\mathrm{Var}(m)$

$$\mathrm{Var}(m) \simeq \left(\frac{2\kappa\langle G^2\rangle}{\langle G^{2+2\kappa}\rangle}\right)^{\frac{1}{\kappa}} (\langle G^2\rangle - 1)\left(\frac{T_c - T}{T_c}\right)^{\frac{1}{\kappa}}, \qquad \text{(D.18)}$$

as shown in equation (3.33).

Bibliography

[1] Jin Yang et al. “Brief introduction of medical database and data mining technology in big data era”. In: *Journal of Evidence-Based Medicine* 13.1 (2020), pp. 57–69.

[2] Elia Morgulev, Ofer H Azar, and Ronnie Lidor. “Sports analytics and the big-data era”. In: *International Journal of Data Science and Analytics* 5 (2018), pp. 213–222.

[3] Yanxia Zhang and Yongheng Zhao. “Astronomy in the big data era”. In: *Data Science Journal* 14 (2015).

[4] Giuseppe Carleo et al. “Machine learning and the physical sciences”. In: *Reviews of Modern Physics* 91.4 (2019), p. 045002.

[5] Pankaj Mehta et al. “A high-bias, low-variance introduction to Machine Learning for physicists”. In: *Physics Reports* 810 (2019). A high-bias, low-variance introduction to Machine Learning for physicists, pp. 1–124. ISSN: 0370-1573. DOI: https://doi.org/10.1016/j.physrep.2019.03.001. URL: https://www.sciencedirect.com/science/article/pii/S0370157319300766.

[6] Giorgio Parisi. *Complex Systems: a Physicist’s Viewpoint*. 2002. arXiv: cond-mat/0205297 [cond-mat.stat-mech].

[7] H Eugene Stanley and Victor K Wong. “Introduction to phase transitions and critical phenomena”. In: *American Journal of Physics* 40.6 (1972), pp. 927–928.

[8] Jack D Cowan, Jeremy Neuman, and Wim van Drongelen. “Wilson–Cowan equations for neocortical dynamics”. In: *The Journal of Mathematical Neuroscience* 6.1 (2016), pp. 1–24.

[9] Victor Amelkin, Francesco Bullo, and Ambuj K Singh. “Polar opinion dynamics in social networks”. In: *IEEE Transactions on Automatic Control* 62.11 (2017), pp. 5650–5665.

[10] Shraddha Gupta et al. “Perspectives on the importance of complex systems in understanding our climate and climate change—The Nobel Prize in Physics 2021”. In: *Chaos: An Interdisciplinary Journal of Nonlinear Science* 32.5 (2022), p. 052102.

[11] G. Lohmann. “Temperatures from energy balance models: the effective heat capacity matters”. In: *Earth System Dynamics* 11.4 (2020), pp. 1195–1208. DOI: 10.5194/esd-11-1195-2020. URL: https://esd.copernicus.org/articles/11/1195/2020/.

[12] Hugh R Wilson and Jack D Cowan. “Excitatory and inhibitory interactions in localized populations of model neurons”. In: *Biophysical journal* 12.1 (1972), pp. 1–24.

[13] Alex Arenas et al. “Modeling the spatiotemporal epidemic spreading of COVID-19 and the impact of mobility and social distancing interventions”. In: *Physical Review X* 10.4 (2020), p. 041055.

[14] M. E. J. Newman. *Networks: an introduction*. Oxford; New York: Oxford University Press, 2010. ISBN: 9780199206650 0199206651.

[15] B. Bollobás. *Random Graphs*. Cambridge Studies in Advanced Mathematics. Cambridge University Press, 2001. ISBN: 9780521809207. URL: https://books.google.com.br/books?id=EX6rQgAACAAJ.

[16] Dunia López-Pintado. “Diffusion in complex social networks”. In: *Games and Economic Behavior* 62.2 (2008), pp. 573–590. ISSN: 0899-8256. DOI: https://doi.org/10.1016/j.geb.2007.08.001. URL: https://www.sciencedirect.com/science/article/pii/S0899825607001157.

[17] Alice Boit et al. “Mechanistic theory and modelling of complex food-web dynamics in Lake Constance”. In: *Ecology Letters* 15.6 (2012), pp. 594–602. DOI: https://doi.org/10.1111/j.1461-0248.2012.01777.x. eprint: https://onlinelibrary.wiley.com/doi/pdf/10.1111/j.1461-0248.2012.01777.x. URL: https://onlinelibrary.wiley.com/doi/abs/10.1111/j.1461-0248.2012.01777.x.

[18] Gustavo Kohlrausch and Sebastián Gonçalves. *Wealth distribution on a dynamic complex network*. 2023. DOI: 10.48550/ARXIV.2302.03677. URL: https://arxiv.org/abs/2302.03677.

[19] Claudio Castellano, Santo Fortunato, and Vittorio Loreto. “Statistical physics of social dynamics”. In: *Rev. Mod. Phys.* 81 (2 May 2009), pp. 591–646. DOI: 10.1103/RevModPhys.81.591. URL: https://link.aps.org/doi/10.1103/RevModPhys.81.591.

[20] Marc Benayoun et al. “Avalanches in a Stochastic Model of Spiking Neurons”. In: *PLOS Computational Biology* 6.7 (July 2010), pp. 1–13. DOI: 10.1371/journal.pcbi.1000846. URL: https://doi.org/10.1371/journal.pcbi.1000846.

[21] Raj Kumar Pathria. *Statistical mechanics*. Elsevier, 2016.

[22] Mark EJ Newman and Gerard T Barkema. *Monte Carlo methods in statistical physics*. Clarendon Press, 1999.

[23] Leo P. Kadanoff. “More is the Same: Phase Transitions and Mean Field Theories”. In: *Journal of Statistical Physics* 137.5-6 (Sept. 2009), pp. 777–797. DOI: 10.1007/s10955-009-9814-1. URL: https://doi.org/10.1007%2Fs10955-009-9814-1.

[24] Wilhelm Lenz. “Beitrag zum Verständnis der magnetischen Erscheinungen in festen Körpern”. In: *Z. Phys.* 21 (1920), pp. 613–615.

[25] Ising Ernst. “Beitrag zur theorie des ferromagnetismus”. In: *Zeitschrift für Physik A Hadrons and Nuclei* 31.1 (1925), pp. 253–258.

[26] Stefan Bornholdt and Friedrich Wagner. “Stability of money: phase transitions in an Ising economy”. In: *Physica A: Statistical Mechanics and its Applications* 316.1-4 (2002), pp. 453–468.

[27] Andrew Lucas. “Ising formulations of many NP problems”. In: *Frontiers in physics* 2 (2014), p. 5.

[28] David Sherrington and Scott Kirkpatrick. “Solvable Model of a Spin-Glass”. In: *Phys. Rev. Lett.* 35 (26 Dec. 1975), pp. 1792–1796. DOI: 10.1103/PhysRevLett.35.1792. URL: https://link.aps.org/doi/10.1103/PhysRevLett.35.1792.

[29] Marc Mezard, Giorgio Parisi, and Miguel Angel Virasoro. *Spin Glass Theory and Beyond: AN Introduction to the Replica Method and its Applications*. 1987. DOI: 10.1142/0271.

[30] Lars Onsager. “Crystal statistics. I. A two-dimensional model with an order-disorder transition”. In: *Physical Review* 65.3-4 (1944), p. 117.

[31] Thomas Vojta. “Rare region effects at classical, quantum and nonequilibrium phase transitions”. In: *Journal of Physics A: Mathematical and General* 39.22 (2006), R143.

[32] Sergey N Dorogovtsev, Alexander V Goltsev, and José FF Mendes. “Critical phenomena in complex networks”. In: *Reviews of Modern Physics* 80.4 (2008), p. 1275.

[33] S. N. Dorogovtsev, A. V. Goltsev, and J. F. F. Mendes. “Ising model on networks with an arbitrary distribution of connections”. In: *Physical Review E* 66.1 (July 2002). DOI: 10.1103/physreve.66.016104. URL: https://doi.org/10.1103%2Fphysreve.66.016104.

[34] M. Leone et al. “Ferromagnetic ordering in graphs with arbitrary degree distribution”. In: *The European Physical Journal B* 28.2 (July 2002), pp. 191–197. DOI: 10.1140/epjb/e2002-00220-0. URL: https://doi.org/10.1140%2Fepjb%2Fe2002-00220-0.

[35] Sander Dommers et al. “Ising Critical Behavior of Inhomogeneous Curie-Weiss Models and Annealed Random Graphs”. In: *Communications in Mathematical Physics* 348.1 (Sept. 2016), pp. 221–263. DOI: 10.1007/s00220-016-2752-2. URL: https://doi.org/10.1007%2Fs00220-016-2752-2.

[36] Fernando L Metz and Thomas Peron. “Mean-field theory of vector spin models on networks with arbitrary degree distributions”. In: *Journal of Physics: Complexity* 3.1 (Feb. 2022), p. 015008. DOI: 10.1088/2632-072x/ac4bed. URL: https://doi.org/10.1088/2632-072x/ac4bed.

[37] Herbert Goldstein. *Classical Mechanics*. Addison-Wesley, 1980.

[38] P Peretto. “Collective properties of neural networks: a statistical physics approach”. In: *Biological cybernetics* 50.1 (1984), pp. 51–62.

[39] Roy J Glauber. "Time-dependent statistics of the Ising model". In: *Journal of mathematical physics* 4.2 (1963), pp. 294–307.

[40] A. C. C. Coolen. *Statistical Mechanics of Recurrent Neural Networks II. Dynamics*. 2000. DOI: 10.48550/ARXIV.COND-MAT/0006011. URL: https://arxiv.org/abs/cond-mat/0006011.

[41] I Neri and D Bollé. "The cavity approach to parallel dynamics of Ising spins on a graph". In: *Journal of Statistical Mechanics: Theory and Experiment* 2009.08 (Aug. 2009), P08009. DOI: 10.1088/1742-5468/2009/08/p08009. URL: https://doi.org/10.1088%2F1742-5468%2F2009%2F08%2Fp08009.

[42] Kazushi Mimura and A C C Coolen. "Parallel dynamics of disordered Ising spin systems on finitely connected directed random graphs with arbitrary degree distributions". In: *Journal of Physics A: Mathematical and Theoretical* 42.41 (Sept. 2009), p. 415001. DOI: 10.1088/1751-8113/42/41/415001. URL: https://dx.doi.org/10.1088/1751-8113/42/41/415001.

[43] Bernard Derrida, Elizabeth Gardner, and Anne Zippelius. "An exactly solvable asymmetric neural network model". In: *Europhysics Letters* 4.2 (1987), p. 167.

[44] Fernando L. Metz and Jeferson D. Silva. "Spectral density of dense random networks and the breakdown of the Wigner semicircle law". In: *Physical Review Research* 2.4 (Oct. 2020). DOI: 10.1103/physrevresearch.2.043116. URL: https://doi.org/10.1103%2Fphysrevresearch.2.043116.

[45] A. C. C. Coolen. *Statistical Mechanics of Recurrent Neural Networks I. Statics*. 2000. DOI: 10.48550/ARXIV.COND-MAT/0006010. URL: https://arxiv.org/abs/cond-mat/0006010.

[46] A. Barrat, M. Barthélemy, and A. Vespignani. *Dynamical Processes on Complex Networks*. Cambridge University Press, 2008. ISBN: 9780521879507. URL: https://books.google.com.br/books?id=TmgePn9uQD4C.

[47] M Kochmański, T Paszkiewicz, and S Wolski. "Curie–Weiss magnet—a simple model of phase transition". In: *European Journal of Physics* 34.6 (Oct. 2013), pp. 1555–1573. DOI: 10.1088/0143-0807/34/6/1555. URL: https://doi.org/10.1088/0143-0807/34/6/1555.

[48] P. C. Martin, E. D. Siggia, and H. A. Rose. "Statistical Dynamics of Classical Systems". In: *Phys. Rev. A* 8 (1 July 1973), pp. 423–437. DOI: 10.1103/PhysRevA.8.423. URL: https://link.aps.org/doi/10.1103/PhysRevA.8.423.

[49] Sz Horvát and Carl D Modes. "Connectedness matters: construction and exact random sampling of connected networks". In: *Journal of Physics: Complexity* 2.1 (Jan. 2021), p. 015008. DOI: 10.1088/2632-072X/abced5. URL: https://dx.doi.org/10.1088/2632-072X/abced5.

[50] Pierre C Hohenberg and Bertrand I Halperin. “Theory of dynamic critical phenomena”. In: *Reviews of Modern Physics* 49.3 (1977), p. 435.

[51] HK Janssen, B Schaub, and B Schmittmann. “New universal short-time scaling behaviour of critical relaxation processes”. In: *Zeitschrift für Physik B Condensed Matter* 73 (1989), pp. 539–549.

[52] M Kochmański, T Paszkiewicz, and S Wolski. “Curie–Weiss magnet—a simple model of phase transition”. In: *European Journal of Physics* 34.6 (Oct. 2013), p. 1555. DOI: 10.1088/0143-0807/34/6/1555. URL: https://dx.doi.org/10.1088/0143-0807/34/6/1555.

[53] Pasquale Calabrese and Andrea Gambassi. “Ageing properties of critical systems”. In: *Journal of Physics A: Mathematical and General* 38.18 (2005), R133.

[54] Géza Ódor. “Universality classes in nonequilibrium lattice systems”. In: *Reviews of modern physics* 76.3 (2004), p. 663.

[55] Seventh Edition. “Table of Integrals, Series, and Products”. In: (2007).

[56] Amir Dembo, Eyal Lubetzky, and Yumeng Zhang. “Empirical Spectral Distributions of Sparse Random Graphs”. In: *In and Out of Equilibrium 3: Celebrating Vladas Sidoravicius*. Ed. by Maria Eulália Vares et al. Cham: Springer International Publishing, 2021, pp. 319–345. ISBN: 978-3-030-60754-8. DOI: 10.1007/978-3-030-60754-8_15. URL: https://doi.org/10.1007/978-3-030-60754-8_15.

[57] Pasquale Calabrese and Andrea Gambassi. “Ageing properties of critical systems”. In: *Journal of Physics A: Mathematical and General* 38.18 (2005), R133.

[58] F. L. Metz, G. Parisi, and L. Leuzzi. “Finite-size corrections to the spectrum of regular random graphs: An analytical solution”. In: *Physical Review E* 90.5 (Nov. 2014). DOI: 10.1103/physreve.90.052109. URL: https://doi.org/10.1103%2Fphysreve.90.052109.